HHS Public Access

Author manuscript

Brain Behav Immun. Author manuscript; available in PMC 2023 March 01.

Published in final edited form as:

Brain Behav Immun. 2022 March ; 101: 246–263. doi:10.1016/j.bbi.2022.01.016.

Sex-dependent pain trajectories induced by prolactin require an inflammatory response for pain resolution

Jennifer Mecklenburg[1], **Andi Wangzhou**[6], **Anahit H. Hovhannisyan**[1], **Priscilla Barba-Escobedo**[1], **Sergey A. Shein**[2], **Yi Zou**[4], **Korri Weldon**[4], **Zhao Lai**[4,5], **Vincent Goffin**[7], **Gregory Dussor**[6], **Alexei V. Tumanov**[2], **Theodore J. Price**[6], **Armen N. Akopian**[1,3]

[1]Department of Endodontics, the School of Dentistry, University of Texas Health Science Center at San Antonio (UTHSCSA), San Antonio, Texas 78229

[2]Department of Microbiology, Immunology & Molecular Genetics, the School of Medicine, UTHSCSA, San Antonio, Texas 78229

[3]Department of Pharmacology, the School of Medicine, UTHSCSA, San Antonio, Texas 78229

[4]Department of Molecular Medicine, the School of Medicine, UTHSCSA, San Antonio, Texas 78229

[5]Greehey Children's Cancer Research Institute, UTHSCSA

[6]Department of Neuroscience and Center for Advanced Pain Studies, University of Texas at Dallas (UTD), Richardson TX 75080

[7]Inserm U1151, Université Paris Descartes, Paris, France

Abstract

Pain development and resolution patterns in many diseases are sex-dependent. This study aimed to develop pain models with sex-dependent resolution trajectories, and identify factors linked to resolution of pain in females and males. Using different intra-plantar (i.pl.) treatment protocols with prolactin (PRL), we established models with distinct, sex-dependent patterns for development and resolution of pain. An acute PRL-evoked pain trajectory, in which hypersensitivity is fully resolved within 1 day, showed substantial transcriptional changes after pain-resolution in female and male hindpaws and in the dorsal root ganglia (DRG). This finding supports the notion that

Corresponding author: Armen N. Akopian, PhD, The School of Dentistry, University of Texas Health Science Center @ San Antonio 7703 Floyd Curl Drive, San Antonio, TX 78229-3900, Office: (210) 567-6668 Fax: (210) 567-3389 Akopian@UTHSCSA.edu.

Authorship contribution statement:

J. Mecklenburg, P. Barba-Escobedo, A. Wangzhou, A. H. Hovhannisyan, Y. Zou, D. Garcia, Z. Lai, A. Tumanov and A.N. Akopian: *methodology, investigation, visualization*. A. Wangzhou, Y. Zou, Z. Lai, G. Dussor, S.A. Shein, A.V. Tumanov, T. J. Price and A.N. Akopian: *analysis, conceptualization*. Vincent Goffin, G. Dussor, T. J. Price and A.N. Akopian *research design*. G. Dussor, A. Tumanov, T. J. Price and A.N. Akopian: *resources, supervision, funding acquisition, manuscript preparation*.

Competing interests:

All authors declare that they have no known competing financial interests or personal relationships that could influence the work reported in this manuscript.

pain resolution is an active process. Prolonged treatment with PRL high dose (1μg) evoked mechanical hypersensitivity that resolved within 5–7 days in mice of both sexes and exhibited a pro-inflammatory transcriptional response in the hindpaw, but not DRG, at the time point preceding resolution. Flow cytometry analysis linked pro-inflammatory responses in female hindpaws to macrophages/monocytes, especially $CD11b^+/CD64^+/MHCII^+$ cell accumulation. Prolonged low dose PRL (0.1μg) treatment caused non-resolving mechanical hypersensitivity only in females. This effect was independent of sensory neuronal PRLR and was associated with a lack of immune response in the hindpaw, although many genes underlying tissue damage were affected. We conclude that different i.pl. PRL treatment protocols generates distinct, sex-specific pain hypersensitivity resolution patterns. PRL-induced pain resolution is preceded by a pro-inflammatory macrophage/monocyte-associated response in the hindpaws of mice of both sexes. On the other hand, the absence of a peripheral inflammatory response creates a permissive condition for PRL-induced pain persistency in females.

Keywords

sex-difference; pain resolution; inflammation; prolactin; skin; DRG

1 Introduction:

Many inflammatory and idiopathic chronic pain conditions, such as migraine, fibromyalgia, temporomandibular disorders (TMJD), irritable bowel syndrome (IBS), and rheumatoid arthritis, have 2–6-fold greater prevalence and/or intensity in women as compared to men (Berkley, 1997; Fillingim et al., 2009; Traub and Ji, 2013; Unruh, 1996). These differences could be explained by distinct pain mechanisms for women and men (Mogil, 2020). These distinctions could be due to variations in pathways involved in nociception, as well as specific mechanisms controlling the development and maintenance of chronic pain conditions (Mogil, 2020; Price and Ray, 2019).

Despite an emerging wealth of information on signaling mechanisms, relatively little is known about sex-specific mechanisms controlling chronic pain initiation, or pain resolution. In this respect, several possibilities were suggested. Spinal microglia and/or dorsal root ganglion (DRG) macrophages, which are involved in chronic pain initiation (Chen et al., 2018), are currently thought to promote chronic pain in males, but not females (Sorge et al., 2015; Yu et al., 2020). In contrast, T-cells are linked to initiation of chronic pain in a female-selective fashion (Sorge et al., 2015), although they are also linked to pain resolution in both sexes (Durante et al., 2021; Krukowski et al., 2016; Laumet et al., 2019). Another neuro-immune mechanism for chronic pain resolution in chemotherapy-induced neuropathy (CIPN) involves IL-23/IL-17A/TRPV1 signaling (Luo et al., 2021). Sex hormones signaling via nuclear receptors could be key contributors to sex-dependent mechanisms of initiation and resolution of chronic pain conditions (Fillingim et al., 2009; Mogil, 2020; Traub and Ji, 2013). Thus, deletion of estrogen receptor subunit α in $TRPV1^+$ nociceptors eliminate IL-23- and IL-17-induced pain in females (Luo et al., 2021). Moreover, treatment of female mice with testosterone promotes microglial-driven pain signaling that is normally absent in females (Sorge et al., 2015).

Two important genes regulated by sex hormones are prolactin (PRL) and its receptor (PRLR). PRL and PRLR regulation by estrogen receptors is well documented (Diogenes et al., 2006; Freeman et al., 2000; Patil et al., 2019b; Utama et al., 2006). However, it is not clear whether the expression of these genes is controlled by testosterone. On another hand, PRL can modulate testosterone secretion in both the pituitary and testis (Sanford and Baker, 2010). PRL is released by pituitary and extra-pituitary tissues during injuries and trauma (Freeman et al., 2000; Marano and Ben-Jonathan, 2014; Scotland et al., 2011). This release of PRL has sex-dependent effects on nociception and sensory neuron sensitization due to differential expression of PRLR in females versus male sensory neurons (Patil et al., 2019b; Patil et al., 2014; Patil et al., 2013). As a result of PRL-induced transient sensitization of sensory neurons, ablation of PRLR on DRG neurons sex-dependently reduces hypersensitivity in acute pain models/conditions (Patil et al., 2019a). These neuronal mechanisms likely depend on the short isoform of prolactin receptor (PRLR-S) (Belugin et al., 2013; Chen et al., 2020). In contrast to PRLR-S, the PRLR long isoform (PRLR-L), which is produced from the same gene (Kelly et al., 1991), is able to activate STAT5 (pSTAT5) pathways leading to expression changes in cells and causes cellular plasticity (Ben-Jonathan et al., 2008). While there is a strong basis for the PRL system contributing to acute pain conditions, there are also findings on a pain inhibitory role for PRL, in particular when it is elevated for a long time and likely acting via PRLR-L. For instance, PRL undergoes natural, prolonged, and substantial elevation during pregnancy, and this could contribute to reported pain inhibition and delayed development during last trimester of pregnancy (Rosen et al., 2017). Moreover, prolonged PRL treatments of already established inflammatory conditions can lead to pain resolution in males (Adan et al., 2013).

These observations on a dual role of PRL in modulation of pain were the rationale for doing the evaluating the hypothesis of whether prolonged local treatments with PRL could have a sex-dependent effect on pain initiation and/or resolution. Given the paucity of information on female chronic pain mechanisms, the disproportionate propensity to develop chronic pain in women, and a dual effect of PRL, we focused on exogenous PRL as a stimulus (Patil et al., 2019a; Patil et al., 2013); and took advantage of different doses and time courses of treatment that are known to have divergent functional impacts in rodents (Cabrera-Reyes et al., 2019). Accordingly, our aim in this study was to use RNA sequencing to investigate biological processes in the hindpaw and dorsal root ganglia (DRG) using a model system with prolonged/multiple exogenous treatments with different doses of PRL that could lead to different pain trajectories and resolution in male and female mice. Surprisingly, our findings suggest that PRLR on non-neuronal cells sex-dependently contributes to resolution of chronic pain through an inflammatory process. Overall, these experiments give new insight into how PRL promotes chronic pain highlighting the important role that early inflammation plays in pain resolution.

2. Materials and Methods:

2.1 Ethical Approval

All animal experiments comply with the National Institutes of Health guide for the care and use of Laboratory animals (NIH Publications No. 8023, revised 1978). We have also

followed guidelines issued by the Society for Neuroscience (SfN) to minimize the number of animals used and their suffering. All animal experiments conform to protocols approved by the University Texas Health Science Center at San Antonio (UTHSCSA) and University Texas at Dallas (UTD) Animal Care and Use Committee (IACUC). The sex and age of animals are indicated in the text.

2.2. Mouse lines

Eight-to-twelve-week-old female or male C57BL/6 mice were used for all described experiments. The Rosa26$^{LSL\text{-}tDTomato/-}$ mouse line on B6.129 background was obtained from the Jackson Laboratory (Bar Harbor, ME). The *Prlr*$^{cre/-}$ mouse line (*Prlr-cre*) on B6.129 background was made by Dr. Ulrich Boehm (University of Saarland School of Medicine, Homberg, Germany) using homologous recombination in mouse embryonic stem (ES) cells (Candlish et al., 2015). The targeting construct was designed to insert an internal ribosome entry site (IRES) and the sequence for Cre recombinase immediately after exon 10 in the *Prlr* gene, with an FRT-flanked neomycin-resistance cassette for selection of clones. Hence, *Prlr-cre* is driven only by large *Prlr* isoform (Candlish et al., 2015; Patil et al., 2019b). The *Prlr*$^{fl/fl}$ mouse line on B6.129 background was generated and provided by Dr. David Grattan (University of Otago, Otago, New Zealand). This mouse line was previously thoroughly characterized for neurons of the central nervous system and sensory neurons (Brown et al., 2016; Brown et al., 2017; Paige et al., 2020; Patil et al., 2019a). Nav1.8$^{cre/-}$ mouse line was generated and provided by Dr. John Wood (University College London, London, UK). This mouse line was thoroughly characterized by multiple research groups (Stirling et al., 2005).

2.3. Prolactin treatments for RNA-sequencing

For all experiments described here, as in our previous studies, we have used human recombinant prolactin (PRL). Such PRL successfully activates mouse prolactin receptor (PRLR) (Freeman et al., 2000; Patil et al., 2019a). Human PRL is a more effective (more potent EC_{50}) activator of rodent PRLR compare to rat and mouse PRL (Utama et al., 2009). Recombinant human PRL was produced in the laboratory of Dr. Vincent Goffin (Inserm U1151, Université Paris Descartes, Paris, France). Lyophilized PRL shipped from France was dissolved in sterile phosphate buffered saline (PBS) pH 7.2 at a stock concentration of 1 mg/ml.

We have used different mouse groups for RNA-sequencing, immunohistochemistry (IHC), flow cytometry and behavioral experiments. However, the development of mechanical hypersensitivity was monitored in animals used for collections of biopsies for RNA-seq as well as IHC and flow cytometry. Biopsies were collected 4–6 hours after last measurements of mechanical hypersensitivity. L3–L5 DRG was isolated using standard procedures as described previously (Patil et al., 2013). The paw samples were collected using 3mm punch biopsies up to the fat layer deep on the plantar surface of the hindpaws.

We have used the following experimental groups in mice for RNA-sequencing. *First group*: PRL (1μg in 5μl) was injected intra-plantar (i.pl.) into hindpaws of male mice. At 1d post-PRL injection, paw and ipsilateral L3–L5 DRG biopsies were isolated. *Second group*:

PRL (1μg in 5μl) was injected i.pl. for female mice. At 1d post-PRL injection, paw and ipsilateral L3–L5 DRG biopsies were isolated. *Controls for first and second groups*: male or female mice were given single i.pl. injections with 0.9% saline pH 7.2, and paw and ipsilateral L3–L5 DRG biopsies were isolated 1d post-vehicle. *Third group*: PRL (1μg in 5μl) was injected i.pl. once a day for 12 consecutive days to male mice. At 13d post-first PRL injection, paw and ipsilateral L3–L5 DRG biopsies were isolated. *Fourth group*: PRL (1μg in 5μl) was injected i.pl. once a day for 12 consecutive days to female mice and paw and ipsilateral L3–L5 DRG biopsies were isolated at 13d post-first PRL injection. *Fifth group* was processed as the third group, but PRL dosage was 0.1μg. *Sixth group* was processed as the fourth group, but PRL dosage was 0.1μg. *Controls for third-sixth groups*: male or female was injected i.pl. with 0.9% saline pH 7.2 once a day for 12 consecutive days and paw and ipsilateral L3–L5 DRG biopsies were isolated at 13d post-first vehicle injection. Each group had three to four samples from independent mice (n = 3 – 4). To confirm results, for some experiments two independent trials were performed. RNA-Seq studies were performed as described below on all biopsies from plantar parts of hindpaws and L3–L5 ipsilateral DRG from male and female mice.

2.4. RNA seq transcriptomic data generation, analyses, and statistics

Fresh tissues were homogenized in Rn-easy solution (Qiagen) using a Bead Mill Homogenizer (Omni International, Kennesaw, GA). Total RNA was extracted using Qiagen Rn-easy (Universal Mini Kit) as was previously described (Patil et al., 2013). RNA quality and integrity were checked using Agilent 2100 Bioanalyer RNA 6000 Nano chip (Agilent Technologies, Santa Clara, CA). Approximately 500 ng total RNA was used for cDNA library preparation with oligo-dT primers by following the Illumina TruSeq stranded mRNA sample preparation guide (Illumina, San Diego, CA). RNA-seq libraries were subjected to quantification, pooled for cBot amplification and subsequent 50bp single read sequencing run with Illumina HiSeq 3000 platform. Depth of reads was $30–50\times10^6$ bp.

After the sequencing run, de-multiplexing with CASAVA was employed to generate the FastQ files for each sample. The combined raw reads were aligned to mouse genome build mm9/UCSC hg19 using TopHat2 default settings (Trapnell et al., 2009; Trapnell et al., 2012). The BAM files obtained after alignment were processed using HTSeq-count to obtain the counts per gene in all samples (Anders et al., 2015). Then, DESeq-2 was used to identify differentially expressed genes (DEGs) after performing median normalization (Anders and Huber, 2010). Quality control statistical analysis of outliers, intergroup variability, distribution levels, PCA and hierarchical clustering analysis were performed to statistically validate the experimental data. Multiple test correction was performed with Benjamini-Hochberg procedure and adjusted p-value (Padj) was generated. If not specified in the text, criteria for selecting differentially expressing genes (DEGs) were expression levels with RPKM>1, fold-change (FC)>2 and statistically significant DEGs with Padj<0.05. Venn diagrams were generated using https://bioinfogp.cnb.csic.es/tools/venny/ (Mecklenburg et al., 2020). Genes were clustered according to biological processes using the PANTHER software (http://www.pantherdb.org/) (Mecklenburg et al., 2020).

2.5. Data and Material Availability

RNA-seq data has been deposited to GEO Accession numbers are GSE168563 and GSE161826. Supplementary excel files show the raw gene readings/counts per gene for all our sequencing experiments. These supplementary files are “Veh vs 0.1μg PRL-long (Hindpaw; Female)” for RNA-seq from 1d post-PRL hindpaws from females treated by vehicle or 12 consecutive days with 0.1μg PRL i.pl.; “Veh vs 0.1μg PRL-long (Hindpaw; Male)” for RNA-seq from 1d post-PRL hindpaws from males treated by vehicle or 12 consecutive days with 0.1μg PRL i.pl.; “Veh vs 1μg PRL-long (Hindpaw; Female)” for RNA-seq from 1d post-PRL hindpaws from females treated by vehicle or 12 consecutive days with 1μg PRL i.pl.; “Veh vs 1μg PRL-long (Hindpaw; Male)” for RNA-seq from 1d post-PRL hindpaws from males treated by vehicle or 12 consecutive days with 1μg PRL i.pl.; “Veh vs 1μg PRL-long (DRG; Female)” for RNA-seq from 1d post-PRL DRG from females treated by vehicle or 12 consecutive days with 0.1μg PRL i.pl.; “Veh vs 0.1μg PRL-long (Hindpaw; Male)” for RNA-seq from 1d post-PRL hindpaws from males treated by vehicle or 12 consecutive days with 0.1μg PRL i.pl.; “Veh vs 1μg PRL-short (Hindpaw; Female)” for RNA-seq from 1d post-PRL DRG from females treated by vehicle or single 1μg PRL i.pl.; “Veh vs 1μg PRL-short (Hindpaw; Male)” for RNA-seq from 1d post-PRL hindpaws from males treated by vehicle or single 1μg PRL i.pl.;“Veh vs 1μg PRL-short (DRG; Female)” for RNA-seq from 1d post-PRL DRG from females treated by vehicle or single 1μg PRL i.pl.; “Veh vs 1μg PRL-long (DRG; Male)” for RNA-seq from 1d post-PRL DRG from males treated by vehicle or single 1μg PRL i.pl.

2.6. Flow cytometry

Flow cytometry was used to assess immune cell profiles in skin biopsies from female mouse glabrous part of hindpaws. Skin biopsies were collected as described in section 2.3. To eliminate contributions of immune cells from blood, animals were perfused with cold PBS prior to tissue dissections. Single cell suspensions from paw biopsies were generated by treating tissues for 90 min at 37°C with 250 μg/ml Liberase (Millipore-Sigma) and 100 μg/ml dispase I (Millipore-Sigma), washing with Dulbecco’s modified eagle medium (DMEM) containing 5% fetal calf serum (FCS), triturating with Pasteur pipette, and then filtering single-cell suspension through 70μm strainer. Cell suspensions were first stained for viability using Zombie NIR™ Fixable Viability Kit (Biolegend) for 20 min at room temperature in PBS combined with FcR blocking antibody (1 μg, clone 2.4G2, BioXCell) to block non-specific binding. Cells then were washed with 2% FBS/PBS and stained with antibodies against surface antigens for 30 min on ice. Fluorochrome-conjugated antibodies against mouse CD45 (clone 30-F11), CD3 (145-2C11), B220 (RA3-6B2), CD11b (M1/70), CD64 (X54-5/7.1), CD11c (N418), MHC-II (M5/114.15.2), Ly-6G (1A8), Ly-6C (KH1.4) were purchased from BioLegend (San Diego, CA), eBioscience (San Diego, CA) or BD Biosciences (San Jose, CA). Flow cytometry was performed using Celesta or LSRII cytometer (BD Biosciences; San Jose, CA). Data were analyzed using FlowJo LLC v10.6.1 software. Gating strategy to select immune populations in the skin was done as previously described (Yu et al., 2016). Live/CD45^{+} cells were gated using the markers listed below to define cell populations: neutrophils (Nph, CD11b^{+}Ly6G^{+}); macrophages (Mph, CD11b^{+}MHCII^{hi}CD64^{+}); inflammatory Mph (iMph, CD11b^{+}MHCII^{hi}CD64^{+}Ly6C^{+}); monocytes (Mo, CD11b^{+}MHCII^{lo}/SSC^{lo}

CD64^{+}); inflammatory Mo (iMo, CD11b^{+}MHCII^{lo}/SSC^{lo}CD64^{+}Ly6C^{hi}); B cells (B, B220^{+} CD11b^{-}CD11c^{-}); T cells (T, CD3^{+}CD11b^{-}CD11c^{-}) and dendritic cells (DCs, CD11c^{+}CD11b^{+}CD64^{-}).

2.7. Immunohistochemistry

For IHC, we used naïve *Prlr*$^{cre/+}$/*Rosa26*$^{LSL\text{-}tDTomato/+}$ (Prlr/tdTomato) reporter, naïve wild-type and 1d post complete Freund's adjuvant (CFA) treated (i.pl. CFA : PBS = 1 : 1) female and male mice. Glabrous hindpaw skin biopsies from 4% paraformaldehyde perfused mice were isolated as described in *the* section 2.3, post-fixed with 4% paraformaldehyde for 1 hr, cryoprotected with 10% and then 30% sucrose in phosphate buffer overnight, embedded in Neg 50 (Richard Allan Scientific, Kalamazoo, MI); and 30 μm cryo-sectioned. IHC was carried out as previously described (Belugin et al., 2013). The following antibodies were used: anti-PRLR rabbit polyclonal (NSJ Bioreagents; San Diego, CA; catalogue R31199; 1:200) (Patil et al., 2019a); anti-K5 rabbit polyclonal (BioLegend; Cat: 905501; 1:400); anti-vimentin chicken polyclonal (Novus; Cat: NB300-223; 1:400); anti-neurofilament heavy chain (NFH) chicken polyclonal (Bio-Legend; Cat: 822601; 1:3000); anti-CD45 rat monoclonal FITC-conjugated (BioLegend; Cat: 103108; 1:200) and anti-CD11b rat monoclonal FITC-conjugated (BioLegend; Cat: 101206; 1:200). For non-conjugated antibodies, sections were incubated with species appropriate Alexa Fluor secondary antibodies (1:200; Molecular Probes, Eugene, OR). Control IHC was performed on tissue sections processed as described but either lacking primary antibodies or lacking primary and secondary antibodies. Images were acquired using a Keyence BZ-X810 All-in-One Fluorescent Microscope (Keyence, Itasca, IL) or a Nikon Eclipse 90i microscope (Melville, NY, USA) equipped with a C1si laser scanning confocal imaging system. Gain setting was constant during acquisition, and it was established on no primary control slides. Images were processed with NIS-elements software (Nikon Instruments, Melville, NY) or Adobe Photoshop CS2 software. Presented IHC images were from Z-stacks. We have analyzed PRL and CD11b co-expression in the dermal layer of hindpaws of female and male mice treated with saline or CFA. To do so, we captured Z-stacked IHC images using 20X objective from 3 independent tissue sections from 2–4 animals. Then we counted PRL^{+} and CD11b^{+} cells and overlap of these cells in 20X image captures.

2.8. Prolactin-induced pain models and measurement of mechanical hypersensitivity

An appropriate sample size for groups was computed using power analysis (see below). PRL was injected i.pl. into hindpaws. *First and second groups*: PRL (1μg in 5μl) was injected i.pl. for female or male mice and mechanical hypersensitivity was assessed 1d post-PRL. *Controls for first and second groups*: female and male mice were given single i.pl. injections with 0.9% saline pH 7.2, and mechanical hypersensitivity was assessed 1d post-vehicle. *Third and fourth groups*: PRL (1μg in 5μl) was injected i.pl. once a day for 12 consecutive days for female or male mice and mechanical hypersensitivity was measured at different time points indicated in the text. *Controls for third and fourth groups*: female and male were injected i.pl. with 0.9% saline pH 7.2 once a day for 12 consecutive days and mechanical hypersensitivity was measured at different time points indicated as experimental mice. *Fifth and sixth groups*: PRL (0.1μg or 1μg in 5μl) was injected i.pl. once a day for 12 consecutive days for *Prlr*$^{fl/fl}$ (control) and Nav1.8$^{cre/-}$/*Prlr*$^{fl/fl}$ (Prlr conditional knock-out (CKO)) female

mice and mechanical hypersensitivity was measured at different time points indicated in the text. *Controls for fifth and sixth groups*: $Prlr^{fl/fl}$ and Prlr CKO female mice were injected i.pl. with 0.9% saline pH 7.2 once a day for 12 consecutive days and mechanical hypersensitivity was measured at different time points as experimental mice.

Measurement of hindpaw mechanical sensitivity was performed as previously described (Patil et al., 2019a). Mice were habituated for 45–60 minutes and then the baseline readings (three readings per animal) were taken on the right hindpaw using the up-down von Frey filament method (Chaplan et al., 1994). To assess development of mechanical hypersensitivity, mechanical withdrawal thresholds were measured at ipsi- and contralateral hindpaws at the time points specified in the text and shown on figures. Behavior experiments were blinded such that the experimenter was not aware of the treatment conditions. We also used randomized designs for behavioral experiments, in which animals were assigned randomly to various experimental groups. Additionally, each experiment was performed in several trials with small numbers on mice in the groups.

2.9. Statistical analysis:

Power analysis for RNA-seq experiments on tissue biopsy samples identified that a sample size of 3 for each group of mice attains >80% power for each test to detect at least 1.5-fold significant difference (FC) in gene expression with an estimated standard deviation of 0.6 (considering low mouse to mouse variation) with a false discovery rate (FDR) of 0.05 using a Benjamini-Hochberg test assuming that the actual distribution is normal. Power analysis for behavioral experiments identified that a sample size of 5 or 7 (depending on model) for each group of mice achieves >80% power for each test to detect significant difference. GraphPad Prism 8.0 (GraphPad, La Jolla, CA) was used for all statistical analyses of data. Data in the figures are mean ± standard error of the mean (SEM), with “n” referring to the number of animals per group. Differences between groups with one variable were assessed by chi-square analysis with Fisher’s exact test, unpaired *t*-test or regular 1-way ANOVA with Tukey’s post-hoc tests, each column was compared to all other columns. Differences between groups with two variables were assessed by 2-way ANOVA with Bonferroni post-hoc tests. A difference was accepted as statistically significant when $p<0.05$. Interaction F ratios, and the associated p values are reported.

3. Results:

3.1. Development of models with sex-dependent initiation and resolution of pain

To achieve a restricted, local effect of PRL, relatively low doses of PRL were used. Previous studies showed that local intra-plantar (i.pl.) injection of <10μg PRL does not produce systemic absorption (Paige et al., 2020; Patil et al., 2019a). We also have previously shown that locally applied PRL (0.1 μg) produced transient mechanical and heat hypersensitivity for up to 6 hours only in females (Patil et al., 2019a). PRL was administrated i.pl. as a single injection and mechanical hypersensitivity at the hindpaw was assessed with von Frey filaments at 1d post-PRL (Figure 1A). Such treatment with 0.1μg PRL produced no mechanical hypersensitivity in hindpaws of females or males demonstrating that there is no persistent effect of PRL at this dose in either sex (data not shown; (Patil et al., 2019a)).

Increasing the dose of i.pl. PRL to 1μg also did not produce mechanical hypersensitivity at 1d-post PRL in ipsilateral hindpaws of females or males (F (1, 16) = 0.04; P=0.84 for row factor; n=5; Figure 1C).

Transient pain-promoting effects of PRL are mediated via protein kinase C-epsilon (PKCε) (Belugin et al., 2013). To activate the STAT5 pathway, prolonged treatment with PRL could be required. We hypothesized that the extended presence of PRL in the hindpaw could activate transcription (likely via STAT5 pathway) in skin cells and/or DRG, which could result in mechanical hypersensitivity. We mimicked prolonged PRL elevation by daily 1μg PRL i.pl. injection for 12 consecutive days (Figure 1B). Such multiday PRL (1μg) i.pl. injections triggered mechanical hypersensitivity measured 1d after the final PRL administration in ipsilateral hindpaws of females (2-way ANOVA; F (4, 40) = 5.18 for raw factor; P=0.02; n=5; Figure 1D) as well as males (2-way ANOVA; F (4, 40) = 2.56 for raw factor; P=0.054; n=5; Figure 1D). In both female and male mice, prolonged PRL-triggered mechanical hypersensitivity gradually resolved within 5–7d (Figure 1D).

Given the equal magnitude of response to multiple doses of PRL in males and females, we reduced dosage of PRL to 0.1 μg to test the hypothesis that repeated exposure to low level PRL would cause pain responses only in female mice. Consistent with this idea, 12 consecutive daily PRL (0.1μg) i.pl. injections triggered mechanical hypersensitivity after the final PRL administration in the ipsilateral hindpaws of female, but not male mice (2-way ANOVA; F (2, 24) = 4.63; P=0.02 for interaction; F (2, 24) = 8.809; P=0.001 for row factor; n=6; Figure 2A). Moreover, prolonged PRL (0.1μg) triggered female-selective mechanical hypersensitivity in the contralateral hindpaw while there was again no effect in males (F (2, 24) = 3.479; P=0.047 for row factor; n=6; Figure 2B).

Single exposure to PRL-induced mechanical hypersensitivity in hindpaws and the female-selective effect of PRLR for acute pain models for the DRG-spinal cord system are partially mediated by sensory neuronal PRLR (Paige et al., 2020; Patil et al., 2019a). This partial effect of sensory neuronal PRLR was also noted for the head and neck areas in trigeminal pain models (Avona et al., 2021). *Prlr* gene ablation in Nav1.8^{+} neurons only partially reduces the response to dural PRL and calcitonin gene related peptide (CGRP)-induced hypersensitivity (Avona et al., 2021). In the experiments cited above (Avona et al., 2021; Paige et al., 2020; Patil et al., 2019a), *Prlr* was ablated in the Nav1.8^{+} subgroup of sensory neurons, since PRLR expression was mainly (>90–95%) detected in peptidergic Nav1.8^{+} DRG and TG neurons (Avona et al., 2021; Patil et al., 2019b). This indicates that activation of sensory neurons by PRL could be indirect. Accordingly, we examined whether sensory neuronal PRLR contributes to the development of mechanical hypersensitivity after prolonged PRL treatment of female or male skin. Multi-day i.pl. PRL (0.1μg) treatments led to gradual development of persistent and non-resolving (for 46 days) hypersensitivity in ipsilateral hindpaws of Prlr$^{fl/fl}$ (control) female mice (2-way ANOVA; F (9, 80) = 16.88 for row factor; P<0.0001; Figure 2C). Contrary to previous findings with a single exposure to PRL, sensory neuronal PRLR ablation did not reduce mechanical hypersensitivity for the initial 32 days post PRL treatment (2-way ANOVA; F (9, 80) = 3.7 for interaction; P=0.0006; Figure 2C) demonstrating that most of the effect induced by repeated exposure to PRL in female mice is not mediated by sensory neuronal PRLR. Again, aside from

an early hypersensitivity that resolved prior to the last PRL treatment, no mechanical hypersensitivity was seen in male mice lacking PRLR in sensory neurons (Figure 2C). The contralateral effect in female mice was again seen in mice lacking PRLR in sensory neurons (2-way ANOVA; $F(9, 80) = 10.90$; $P<0.0001$ for row factor; Figure 2D); and there was no difference in time to resolution in the sensory neuron PRLR ablated mice for the contralateral paw (2-way ANOVA; $F(1, 80) = 0.9184$; $P=0.3408$ for column factor; Figure 2D). Thus, our behavioral findings demonstrate an acute pain, female-selective effect of low dose PRL that resolves fully within 1d (Figures 1A, 1C); a female-selective, low dose-PRL, non-resolving persistent pain model (Figures 1B, 2C); as well as high dose, more persistent but still rapidly resolving pain trajectory for females (Figure 1D) and males (Figures 1D, 2C). Sensory neuronal PRLR does not contribute to the non-resolving persistent pain effect in females. Finally, the persistent, non-resolving pain trajectory in females likely has a systemic immune or central nervous system (CNS) component since contralateral hindpaw effects were clearly present (Figure 2D).

3.2. Alterations of hindpaw skin and DRG gene expressions by single high dose i.pl. PRL administration

Using the same timeline schematically presented in Figure 1A, mechanical sensitivity at the baseline time point and then 1d post-PRL was monitored prior to obtaining skin and DRG biopsies for RNA-seq. Using RNA-seq data analysis, we evaluated whether a single i.pl. administration of exogenous PRL (1 μg) leads to transcriptomic changes in hindpaw skin samples or in the DRG of males and females at 1d post-PRL, when mechanical hypersensitivity was fully resolved (Figure 1C). Surprisingly, a profound number of DEGs (>1400) were detected in the ipsilateral hindpaw and the L3–L5 DRG, despite pain being fully resolved in both females and males (Figures 1C, 3A, 3B, 4A, 4B). Moreover, these DEGs substantially overlapped for female and male tissue biopsies. We found 66.8% (1212) up-regulated and 73.5% (1617) down-regulated DEGs were common for ipsilateral female and male hindpaw samples (Figures 3A, 3B). For ipsilateral L3–L5 DRG, single PRL exposure produced relatively lower numbers of up-regulated DEGs (134 for females and 157 for males; Figure 4A). In contrast, PRL treatment caused a greater number (1809 for females and 1798 for males) of down-regulated DEGs, a majority of which also overlapped (81.9%; Figure 4B).

PANTHER (http://www.pantherdb.org/) was used to assign biological processes to DEG clusters. In hindpaw, up-regulated DEGs common for females and males were related to metabolic processes, including cellular energy production (*Atp5a1, Atp7a, Cox7a1, Ndufs2, Ndufb5, Ndufa7, Ndufb7, Sdha, Sdhc, Sdhd, Uqcrc1, Uqcrq*, etc.) as well as tissue myofibril assembly (*Ttn, Tnnc1, Tnnc2, Myo5a, Myh8, Mylpf, Myo1d, Myl4, Myl6, Lmod2, Tmod2, Tmod4* etc.) (Figure 3C). A few up-regulated DEGs were specific for females or males, and they represent related biological processes: primary and cellular metabolic processes. A small number of immune responses associated genes were also up-regulated in female and male hindpaw samples (Figure 3C), but a majority of such DEGs were down-regulated including innate immune responses (*Ccl6, Ccl9, Ccl12, Tlr5, Tlr7, Tlr8, Tlr9, Bst2*, etc.); phagocytosis (*Dock7-Dock11*); adaptive immune responses (*Il6ra, Mill2, H2-K1, H2-T23*); and leukocyte activation (*CD80, Tnfrsf14, Fert2, Il6ra*) (Figure 3D). Most genes with

reduced expression in the hindpaw regulate the function of different types of cells, such as epithelial, fibroblasts, endothelial and neurons (Figure 3D).

Up-regulated DEGs in ipsilateral L3–L5 DRG did not fit any specific biological processes in males or females (Figure 4A). On other hand, male-selective, female-selective, and common down-regulated DRG DEGs could be assigned to specific biological processes (Figures 4C, 4D). For instance, female-selective down-regulated DEGs in DRG were mainly related to suppression of immune system processes (Figure 4C). Shared down-regulated DEGs in DRG were linked to suppression of synaptogenesis, axonogenesis and neurogenesis, a variety of metabolic processes and general epigenetic and transcription machinery (Figure 4D). Overall, after full resolution of acute pain induced by single high dose PRL i.pl. injection, large numbers of DEGs in ipsilateral hindpaws and L3–L5 DRG in females and males were still detected. These DEGs were largely associated with down-regulation of immune processes, and up-regulation of tissue/cell development and metabolic processes.

3.3. Alterations of hindpaw skin and DRG gene expression by multiday i.pl. high dose (1 μg) PRL administration

We next examined transcriptomic changes in female and male ipsilateral hindpaws and L3–L5 DRG at 1d post 12-day i.pl. 1 μg daily PRL administration (schematic of experiments in Figure 1B), when mechanical hypersensitivity was present in males and females, but resolved within 5–7 days (Figure 1D). At this time point, relatively smaller numbers of DEGs were found in ipsilateral hindpaw (Figures 5A, 5B) and especially, DRG samples (Figures 6A, 6B). These DEGs have showed substantial sex-dependency compare to DEGs revealed at 1d after single PRL (1 μg) i.pl. administration (Figures 5A, 5B, 6A, 6B vs 3A, 3B, 4B). Fourty-one % (n=296) of up-regulated and only 3% (n=6) of down-regulated DEGs were common for female and male hindpaw skin samples (Figures 5A, 5B), while numbers of DEGs were small in DRG for both females and males (Figures 6A, 6B).

PANTHER analysis revealed that 12-day PRL treatment resulted in events in which a majority of upregulated DEGs in hindpaw skin of females and males are linked to immune system processes (Figures 5C–5E). Female-specific up-regulated DEGs were associated with pro-inflammatory processes (Figure 5C), including lymphocyte and leukocyte activation and proliferation (*Cd3e, Cd33, Cd28, Cd180, Lck, Ctsc, Ctla4, Fap, etc.*), cytokine production (*Csf1r, Tlr7, Fcgr3, etc.*) and the adaptive immune response (*Tcirg1, C1ra, Siglecg, Ctsh, etc.*). Male-specific up-regulated DEGs were also associated with pro-inflammatory processes (Figure 5D), such as lymphocyte and leukocyte differentiation, proliferation, and migration (*Ccr1, Ccl2, Ccl7, Ccl3, Cxcl10, Cx3cr1, Nfkbid, Tnf, Tnfrsf1b, Tnfrsf14, Cd40, Cd80, Cd244, Cd276, Tlr9, Lyn, etc.*). Similarly, common up-regulated DEGs were linked to immune system processes (*H2-D1, H2-K1, H2-Aa, Ptprc, Aif1, Tlr1, Tlr8, Cd4, Cd74, Cd274, Cd300lb, Ccr2, Ccr5, Igf1, Nfam1, Irf4, Irf7, Irf8, Itgal, Vcam1, Vav1, etc.*) (Figure 5E). A few male-specific down-regulated hindpaw skin DEGs were linked to epithelium and epidermis development. However, no gene clusters or biological processes could be assigned to down-regulated female-selective hindpaw skin nor to up-regulated DRG DEGs. *Stat5a* and *Stat5b* genes were not regulated by multi-day treatment with PRL in hindpaw skin and DRG of females and males (Supplementary Material).

Nevertheless, PRL can activate the STAT5 pathway by interaction with PRLR, consequent phosphorylation of STAT5, and translocation of a Jak2/pSTAT5 complex into the nucleus where transcriptional regulation will occur (Freeman et al., 2000; Rani and Murphy, 2016). STAT5 pathway activation by PRL in these experiments is evident in regulation of multiple STAT5 target genes, including the immune system modulating genes and pathways: IL-2, IL-3 and Bcl-2 signaling, *Il2ra*, *Tnfsf10*, *Foxp3, Slfn2, C3ar1, Osm, Socs1*, etc. (Basham et al., 2008; Kanai et al., 2014; Teglund et al., 1998) (Supplementary Excel files/material). In summary, multi-day high dose (1 μg) PRL i.pl. treatment primarily up-regulated pro-inflammatory genes in hindpaw skin. These genes can be classified as involved in antigen presentation, innate and adaptive immunity activations, chemokine and IL-1, IL-2, and IL-6 production. It is notable that although many of these genes are well-known for pro-nociceptive actions (Chen et al., 2018; Yu et al., 2020), they were nevertheless associated with mechanical hypersensitivity that resolved rapidly after stopping 12-day i.pl. PRL treatment.

3.4. Alterations of hindpaw skin gene expression by multiday i.pl. low dose (0.1 μg) PRL injection

Prolonged treatment with low dose (0.1μg) of PRL generated persistent mechanical hypersensitivity only in females (Figure 2A). Importantly, this model represents a non-resolving persistent female-selective pain model, which is sensory neuronal PRLR independent (Figure 2C). Additionally, it could be considered a resolving pain model for males, in which hypersensitivity return to baseline during the course of PRL treatments (Figure 2C). Hence, we examined transcriptomic changes in female and male hindpaws at 1d post-PRL (0.1 μg) multi-day treatment. We did not examine expression changes in DRG because we did not observe changes with multi-day treatment with high dose of PRL. At this time point, unexpectedly, larger numbers of DEGs compared to prolonged (12d) treatment with a higher (1 μg) PRL dosage were found in both female and male hindpaws (Figures 7A, 7B). Moreover, despite divergent pain responses in females and males following PRL treatment with this low dose (Figure 2C), 49.5% of up-regulated and 63.6% of down-regulated DEGs were common for female and male ipsilateral hindpaws. PANTHER analysis showed that common up-regulated genes related to cellular respiration, peptide metabolic, and apoptotic processes (Figure 7D). Down-regulated common DEGs were associated with regeneration and development of a variety of cell types and tissues (Figure 7F). Female-selective up-regulated genes did not fit any specific biological process, while male-selective genes corresponded to the immune system and cellular metabolic processes (Figure 7C). Interestingly, female-selective down-regulated genes revealed only two clusters related to cellular and macromolecule metabolic processes (data not shown). In contrast, cell differentiation and proliferation, axonogenesis and neurogenesis were specifically reduced in male hindpaw samples (Figure 7E). Our findings suggest that the persistent non-resolving pain condition in females was preceded by tissue degeneration gene programs including a suppression of genes for morphogenesis and an absence of up-regulation of DEGs found in males that were associated with tissue repair. In contrast, resolved pain responses at this time point in males exhibited upregulated tissue repair genes, and substantial reduction of neurogenesis and axonogenesis in hind paws that could produce pain (Xie et al., 2017).

Multi-day treatment with 1 μg and 0.1 μg PRL produced different behavioral effects in males and females (Figures 1D vs 2C). Therefore, we compared gene expressions in ipsilateral hindpaw samples for these doses at 1d post-PRL treatment in females and males. Expectedly, overlap for these models in females were low for both up- and down-regulated DEGs (Figures 8A, 8B). Hindpaws in pain model generated with multi-day 1 μg PRL injection were enriched with up-regulated pro-inflammatory genes (Figure 8C), while the 0.1 μg PRL treatment exhibited down-regulation of multiple genes responsible for tissue regeneration and repair (Figure 8D). Two clusters of primary and peptide metabolic process genes were up regulated in the 0.1 μg PRL treatment group (*data not shown*), but their numbers were substantially lesser than down regulated metabolic process genes (Figure 8D). Our results support the conclusion that pain resolution is linked to elevation of pro-inflammatory genes, which likely support regeneration processes associated with pain resolution.

A similar comparison in male mice also exhibited differences in DEGs profiles between multi-day treatment with 1μg and 0.1μg PRL (Figures 8E, 8F). At 1d post i.pl. treatment with 0.1μg PRL, a time point where mechanical hypersensitivity was fully resolved, we observed up- and down-regulated DEGs (Figures 8G, 8H). These included, metabolic processes, cell development and differentiation, tissue & organ morphogenesis, and neurogenesis and axonogenesis. At 1d post last i.pl. treatment with 1μg PRL, a time point just prior to pain resolution in male mice, up-regulated genes were mainly pro-inflammatory (Figure 8I), while no clear biological events could be assigned to down-regulated DEGs. These findings from male hindpaw biopsies confirm are consistent with the observation in female mice that pain resolution is preceded by elevation of pro-inflammatory genes.

3.5. Changes in immune cell profiles in female hindpaw skin by single and multiple i.pl. PRL injections

Since accumulation of immune cells (i.e. $CD45^+$ cells) into hindpaw skin could contribute to expression changes of immune related genes, we examined whether immune cell profiles were altered by PRL treatment. To do so, we used flow cytometry to examine immune cell profiles after single (1d) and multiple (12d) i.pl. 0.1 μg or 1 μg PRL treatments. Controls were single or multiday i.pl. PBS injections. The detailed gating strategies for live singlets and distinct types of immune cells are depicted in Figure 9.

In concordance with RNA-seq data (Figure 3D), single i.pl. injection of PRL (1 μg) substantially reduced $CD45^+$ cells and macrophages (Mph; $CD11b^+/CD64^+$ cells) in female hindpaws at 1d post-PRL (2-way ANOVA; $F(8, 54) = 49.21$ for row factor; $P<0.0001$; n=4; Figures 10A, 10E). These reductions of $CD45^+$ cell numbers took place despite an increase in monocytes (Mo) and inflammatory monocytes (iMo) (2-way ANOVA; $F(7, 48) = 26.25$ for row factor; $P<0.0001$; n=4; Figure 10B). Up-regulation of pro-inflammatory related genes in female hindpaws after multi-day i.pl. PRL (1μg) treatment led to significant elevation of $CD45^+$ cells, Mph and inflammatory Mph (iMph; 2-way ANOVA; $F(8, 54) = 120.4$ for row factor; $P<0.0001$; n=4; Figures 10C, 10E). This increase in $CD45^+$ cells was due to infiltration into or proliferation in the paw of Mph, iMph as well as iMo, but not dendritic (DCs), B-cells (B), T-cells (T) or neutrophils (Nph) (2-way ANOVA; $F(7, 48) =$

46.72 for row factor; P<0.0001; n=4; Figure 10D). These data indicate that accumulation of monocytes into PRL-treated hindpaw skin of female mice contributes to regulation of DEGs related to immune processes after multiday PRL (1 μg) treatments (Figure 5). Unlike multi-day i.pl. injections with 1 μg PRL, prolonged treatment with low dose PRL (0.1μg) did not increase pro-inflammatory genes in female hindpaws (Figure 7). Consistently, immune cells were not increased in female hindpaws after 12-day-long 0.1 μg PRL i.pl. treatment (2-way ANOVA; F (7, 56) = 53.97 for row factor; P<0.0001; n=4–5; Figures 10F, 10G). Additionally, no-to-low iMph and iMo were found in hindpaw samples from low dose PRL treated female mice (Figures 10F, 10G) compared to marked increase of these cell populations after high dose of PRL treatment (Figures 10C, 10D). These experiments indicate that the increased inflammatory gene expression detected preceding pain resolution is likely due to accumulation (via migration and/or proliferation) of pro-inflammatory and a subset of $CD11b^+$ cells, such as iMph, Mph, iMo and Mo in hindpaw skin of female mice.

3.6. PRLR expression in hindpaw skin cells of females and males

We have previously characterized *Prlr* mRNA expression in DRG and spinal cord cells of female and male mice (Patil et al., 2019a; Patil et al., 2019b). Here we examined what type of cells in female and male skin express PRLR, which can respond to exogenous PRL. *Prlr* mRNA expression in skin cells was assessed in reporter $Prlr^{cre/-}/Rosa26^{LSL\text{-}tDTomato/-}$ naïve female and male mice showing *Prlr*-cre^+ cells. Labeling of cryo-sections of skin from these reporter female and male mice with a variety of markers of non-neuronal cells revealed *Prlr*-cre^+ cell types. Three independent mice were characterized. *Prlr*-cre^+ cell types were reliably defined when labeling was consistent in all three mice.

In female mice, *Prlr*-cre^+ cells did not overlap with resident dermis $CD45^+$ immune cells (yellow arrows; Figures 11A, 11A'). *Prlr*-cre^+ cells were also lacking $CD11b^+$ cells (data not shown). *Prlr*-cre was expressed by a subset of dermis vimentin positive (Vim^+) fibroblasts; a cyan arrow marked Vim^+/*Prlr*-cre^+ and white arrows showed Vim^+/*Prlr*-cre^- cells (Figures 11B, 11B'). Strong *Prlr*-cre expression was also revealed in sweat gland epithelial cells (a blue arrow; Figures 11B, 11B').

In male mice, *Prlr*-cre labeling was absent from dermis layer immune cells, including $CD11b^+$ cells (yellow arrows; Figures 11C, 11C'). *Prlr*-cre signal was at high levels in dermis capillary vessels (a blue arrow; Figure 11C). Like in females, epidermal basal layer of $K5^+$ keratinocytes as well as other keratinocyte types were *Prlr*-cre negative. However, certain epidermal Merkle-like cells contained *Prlr*-cre in females and males. *Prlr*-cre was expressed in sweat gland epithelial cells. Also consistent with female mice, *Prlr*-cre labeling was detected in a subset of dermis Vim^+ fibroblasts (light blue arrows; Figures 11D, 11D'). Like in females, *Prlr*-cre was absent from certain Vim^+ fibroblasts located near the epidermis layer and from melanocytes of the epidermis layer (pink arrows; Figures 11D, 11D'). Overall, *Prlr*-cre, which reflects *Prlr-L* mRNA expression (Candlish et al., 2015), was not sex-dependent and was predominantly expressed in non-immune skin cell types: a subset of fibroblasts, sweat gland epithelial and blood vessel endothelial cells, and epidermis, including Merkel-like cells.

Although we did not observe a baseline sex difference of *Prlr* mRNA in hindpaw cells, treatment with PRL produced dramatic behavioral sex differences (Figure 2C). A possible explanation is that PRLR expression in hindpaws change during inflammation in a sex-specific fashion (Patil et al., 2013). Our previous observations showed that PRL treatment changes monocyte/macrophage profiles with infiltration/proliferation of iMo and iMph (Figure 10). To test this hypothesis, we treated mice with complete Freund's adjuvant (CFA) injection into the hindpaw, which is known to promote infiltration/proliferation of iMph, iMo, Mo, and to lesser extend Mph and Nph (Ghasemlou et al., 2015). We then examined PRLR protein expression in female and male hindpaws at 1d post-treatment with CFA. PRLR was expressed in female and male epithelial cells of hair follicles and in the epidermis layer (white arrows, Figures 12A, 12A", 12B, 12B"). It was also detected in endothelial cells. Importantly, expression of PRLR in $CD11b^+$ cells was sex-dependent after CFA treatment. We manually counted numbers of $CD11b^+$ and $CD11b^+/PRLR^+$ cells in the field of view for images obtained with a 20X objective. These data were accumulated and then averaged from 2–4 images captured from each of 3 mice. The number of $CD11b^+$ cells in the field of view of dermis were approximately equal in females versus males (203±32.7 in females; 218.7±21.68 in males, n=3). However, in females, the percentage of $CD11b^+/PRLR^+$ was low (22.1±2.8%) and these $CD11b^+$ cells expressed PRLR similar to background levels (Figures 12A–12A"). In contrast, there were substantial numbers of $CD11b^+/PRLR^-$ cells (cyan arrows, Figure 12A), and strong PRLR expressing $CD11b^-/PRLR^+$ cells (yellow arrows, Figures 12A, 12A") in female hindpaw dermis. The $PRLR^+$ cells had a fibroblast-like morphology. In males, many $CD11b^+/PRLR^+$ cells (78.4±4.3%) were detected after CFA (blue arrows, Figures 12B–12B") but a substantial number of $CD11b^-/PRLR^+$ cells could still be observed (yellow arrow, Figures 12B, 12B"). This finding demonstrates that CFA-induced inflammation significantly increased PRLR expression in male compare to female skin (*t*-test unpaired; t=11.97, df=4; P=0.0003; n=3) and this increase occurs mostly in a subset of $CD11b^+$ cells that appeared in males during inflammatory conditions.

4 Discussion:

Many forms of chronic pain conditions are more pronounced either in women or in men, but more often in women (Fillingim et al., 2014; Fillingim et al., 2009). There could be two possible explanations for this clinical finding: sex differences in mechanisms regulating the transition to a chronic pain state and/or sex differences in resolution of pain mechanisms. Despite a wealth of information on sex-dependent regulation of many proteins such as G-protein coupled and toll-like receptors (Agalave et al., 2021; Mogil et al., 2003; Rudjito et al., 2021; Sorge et al., 2011), signaling molecules (Berta et al., 2016; Joseph et al., 2003; Khomula et al., 2017; Paige et al., 2018) and neuropeptides like CGRP (Avona et al., 2019; Avona et al., 2021; Chow et al., 2018; Liu et al., 2020) in the nociceptive pathway, mechanisms regulating the transition to chronic pain states and pain resolution in females and males remain largely unknown. One of reasons for slow progress in this issue is the absence of pain models showing clear differences in pain resolution in females versus males. Studying effects of prolonged treatment with PRL on the development of pain conditions, we developed a model in which long-term exposure to low dose of PRL

creates a non-resolving chronic pain state selectively in female mice. We embarked on these studies, since the literature hints to differential actions of PRL depending on treatment time and dosage. There is a consensus that prolonged elevation of PRL activates PRLR-L, which phosphorylates STAT5 (pSTAT5) and causes transcriptional changes in both non-neuronal cells and neurons (Anderson et al., 2006; Bole-Feysot et al., 1998b); while transient increase in PRL could activate both PRLR-L and PRLR-S (Belugin et al., 2013). Activation of PRLR-S in sensory neurons leads to female-selective sensitization and regulation of hypersensitivity in acute pain models (Avona et al., 2021; Patil et al., 2019a; Patil et al., 2013). This transient effect of PRL cannot explain inhibition of pain conditions during the third trimester of pregnancy, when PRL is naturally substantially elevated for a long period (Rosen et al., 2017). This transient effect of PRL cannot also explain the observed inhibition inflammatory pain by prolonged treatment with PRL (Adan et al., 2013). Altogether, we have described a female-specific non-resolving pain model, which is independent of sensory neuronal PRLR, and gives an opportunity to understand sex differences in pain development trajectory, post-resolution cell plasticicity and especially, pain resolution mechanisms in females.

Full resolution of pain likely does not equal a complete returning to pre-pain conditions. It is now well known that even after full resolution of mechanical and thermal pain hypersensitivity, the nociceptive pathway remains primed in a state referred to as “hyperalgesic priming” where treatment with normally sub-threshold doses of pro-nociceptive agents such as bradykinin or prostaglandins can rekindle a pain state (Aley et al., 2000). Hence, it is not surprising that RNA sequencing of hindpaw and DRG samples from females and males collected after hypersensitivity was fully recovered 1d after single PRL treatment revealed a substantial number of DEGs. These DEGs were similar in females and males and were balanced between up-and down-regulated genes in the hindpaw. In the DRG DEGs were almost entirely downregulated and involved in inflammatory, metabolic, neurogenesis and axonogenesis biological processes. In previous publications, it was suggested that post-resolution cell plasticity could depend on the pain condition from which the resolution occurred (Aley et al., 2000; Joseph et al., 2003; Melemedjian et al., 2010). In multi-day 0.1 μg PRL treatment in male mice, sequencing was done at a time point where pain was also completely resolved. Despite we again observed a balance between up- and down-regulated genes, and down-regulation of neurogenesis and axonogenesis DEGs, we also noted a distinction that few inflammatory genes were still up-regulated in the prolonged PRL treatment paradigm in males. In the current study, we did not compare differences in hindpaw and DRG at post-resolution time points after the prolonged pain condition in females. However, substantial differences between females and males at post-resolution time points after longer lasting hypersensitivity could be hypothesized as hyperalgesic priming shows marked sexual dimorphisms that depend on estrogen (Joseph et al., 2003; Paige et al., 2020). Altogether, our data confirm that many changes in gene expression can be found even at post-resolution time points. Moreover, the treatment paradigm, or type of pain condition, contributes to persistent cell plasticity at post-resolution time points. Finally, these gene expression changes appear to balance immune and neuronal processes that may create a new homeostatic set-point.

Multi-day PRL treatment produced either resolving or non-resolving pain phenotypes depending on mouse sex and PRL dose. These PRL multi-day treatments induced substantially different sets of DEGs in females and males compared to single PRL injection protocol. Only approximately 20 common genes were up-regulated by both single and multi-day PRL treatments and they did not fit into any clear biological process. A key conclusion from analysis of resolving and non-resolving mechanical hypersensitivity caused by PRL treatments is that a pro-inflammatory gene expression response in the hindpaw precedes pain resolution (Figures 5C–5E). This pro-inflammatory response revealed by RNA-seq analysis correlates with infiltration or proliferation of myeloid $CD11b^+/CD64^+$ cells in the hindpaw. Another feature non-resolving pain induced by PRL in female is that expectedly, persistent pain leads to development of central sensitization (Woolf, 2011). This central sensitization is likely not due to systemic effect of PRL, since we have used peripheral doses of PRL (<10 μg) (Avona et al., 2021; Patil et al., 2019a). Interestingly, at the late stages of PRL-induced persistent pain (> 30d post-PRL), neuronal PRLR is involved (Figure 2). There is no explanation to this phenomenon, but it is likely related to endogenous PRL, since exogenous PRL could have long been degraded. We also do not have information (and hypothesis) on mechanisms maintaining pain state, and whether these mechanisms sex-dependent, peripheral and/or central and depending on inflammatory mediators. To clarify these issues, detailed RNA-seq in these time points for several tissues in females and males could be done. In summary, our analysis points to several hallmarks of low dose PRL-induced non-resolving pain condition in female mice: 1) very low numbers of up-regulated immune processes related genes, 2) many down-regulated genes responsible for morphogenesis and development, 3) up-regulation of genes regulating axonogenesis and neurogenesis; 4) up-regulation of apoptotic processes and cellular respiration machinery genes; and 5) development central sensitization which becomes sensory neuronal PRLR dependent at later stages (> 30d post-PRL; Figures 2C, 2D).

A key finding emerging from our study is that female mice that showed non-resolving pain did not develop an inflammatory response to prolonged PRL treatment whereas male and female mice with resolving pain did mount such a response. It is widely understood that pro-inflammatory reactions exacerbate pain and could convert acute pain to a chronic pain state (Sommer et al., 2018; Staff et al., 2019). Moreover, it has also been reported that inflammation prevents pain resolution wherein inflammation resolution can be promoted in females by blocking IL-23/IL-17A signaling in macrophages (Luo et al., 2021). Previous studies also show that resolution of inflammatory and other forms of pain could be blocked by removing or inhibiting $CD8^+$ T-cells in DRG controlling IL-10 and IL-4 signaling. Thus, IL-10 and IL-4 in DRG play a key role in resolution of inflammation and resolution of pain (Durante et al., 2021; Eijkelkamp et al., 2016; Krukowski et al., 2016; Willemen et al., 2014). It could be noted that in the 1 μg PRL injection paradigm, where pain resolved in both sexes, overall IL-4 and IL-10 expression levels is low in hindpaws and almost non-existing in DRG. Thus, mean values of Veh versus PRL are IL-4 (0 vs 0 reads) and IL-10 (0 vs 0.04 reads) for male DRG; IL-4 (0 vs 0 reads) and IL-10 (0.28 vs 0 reads) for female DRG; IL-4 (0.52 vs 2.47 reads) and IL-10 is (4.08 vs 13.83 reads; $pval=0.03$) for male paw; and IL-4 (0.95 vs 3.38 reads) and IL-10 is (4.85 vs 24.59 reads; $pval=0.03$) for male DRG (see Supplementary information). Despite reported negative actions of pro-inflammatory

processes on resolution, it could be noted that recovery from tissue damage is a primary biological event leading to pain resolution and that this is an active process requiring involvement of immune cells (Aitcheson et al., 2021). Thus, this pro-inflammatory step may be followed by secretion of TGF-β and promotion of tissue damage repair (Wang et al., 2021). Our data also show that a non-resolving pain condition was accompanied by down-regulation of genes responsible for morphogenesis and development, which play key roles in tissue repair. Considering these points, our data add important nuance to the interplay of pain resolution and inflammation pointing out that escalation of the pro-inflammatory responses accompanied by infiltration or proliferation of $CD11b^+/CD64^+$ cells correlate with pain resolution (Figures 2C, 5, 10). Consistent with our results, it was reported that blockage of CCR2 signaling interfering with $CD11b^+/CD64^+$ cell migration prevents pain resolution in carrageenan-induced inflammatory models (Willemen et al., 2014). Inflammation linked gene upregulation in mice with pain resolution is also consistent with the known roles of resolvins and other inflammation resolution factors in restricting the duration of pain hypersensitivity (Ji et al., 2011).

Our findings also point to a long suspected dual role of the PRL system in many biological processes, including pain (Adan et al., 2013; Avona et al., 2021; Bole-Feysot et al., 1998a; Freeman et al., 2000; Patil et al., 2019a). Prolonged exposure of tissues to PRL leads to inflammation, and this process is more effective in males. PRL is a capable activator of endothelial cells, epithelial cells and fibroblasts, which express PRLR in males and females (Bole-Feysot et al., 1998a; Freeman et al., 2000). Our findings indicate that activation of these type of cells produces a transcriptional state resembling tissue damage. This tissue damage activates the immune system, and PRL amplifies these responses more in males than females, likely because PRLR expression on $CD11b^+$ cells during inflammatory conditions is higher in males (Figure 12). This model is consistent with a pro-inflammatory function of PRL reported in many previous studies (Bole-Feysot et al., 1998b; Brand et al., 2004; Carreno et al., 2004; De Bellis et al., 2005; Dimitrov et al., 2004) that has mostly been attributed to PRLR expression in immune cells during autoimmune and other inflammatory conditions (Borba et al., 2019; Brand et al., 2004; De Bellis et al., 2005). This proposed sequence of events suggests that prolonged treatment by PRL or natural elevation of PRL during pregnancy could speed resolution of existing pain conditions and play a protective effect in development of pain from childbirth (Adan et al., 2013; Rosen et al., 2017). Somewhat paradoxically, our data imply that this protective PRL effect will be more effective in males, and consequently some pain states could emerge more frequently in females due to ineffective inflammation driven pain resolution, which is likely controlled by sex hormones, including PRL.

5. Conclusions:

Overall, these experiments give new insight into how PRL promotes chronic pain highlighting the important role that early inflammation plays in pain resolution. We also reach the following conclusions from our experiments. 1) Different PRL doses and treatment durations generate sex-dependent pain trajectories. 2) RNA sequencing experiments of tissues following complete pain resolution show that there are substantial changes in gene expression supporting the hypothesis that pain resolution is an active process (Aley et al.,

2000; Price et al., 2018). 3) Pain resolution is preceded by a strong pro-inflammatory response in females and males linked in females to a rise of myeloid, especially $CD11b^+$/$CD64^+$/$MHCII^+$ cells at the site of injury. However, further analysis of $CD11b^+$/$CD64^+$ cells will be necessary to delineate distinct macrophage subpopulations induced in the hindpaw of males and females prior to pain resolution. 4) In females, non-resolving pain induced by PRL is associated with upregulation of genes related to tissue damage, but a lack of change in tissue repair pathways giving new insight into why pain may not resolve in certain clinical situations. 5) Finally, cellular anabolism and cellular respiration processes, which were upregulated in hindpaw samples from mice with pain resolution, are known to contribute to recovery from tissue damage by cell regeneration, proliferation and differentiation (Dominguez-Andres et al., 2019; Lampert and Gustafsson, 2019).

Supplementary Material

Refer to Web version on PubMed Central for supplementary material.

Acknowledgements:

We would like to thank Mrs. Dawn Garcia for assistance in performance of the RNA-seq experiments, which were conducted in the Genome Sequencing Facility (GSF) in the Greehey Children's Cancer Research Institute (GCCRI) of UTHSCSA; Dr. Michael Henry for guidance on IHC; Dr. Florence Boutillon for help in synthesizing recombinant human PRL; Dr. Ulrich Boehm (Saarland University School of Medicine, Homburg, Germany) for kindly providing $Prlr^{cre/-}$ reporter mice; and Dr. David Grattan (Otago University, Otago, New Zealand) for kindly providing $Prlr^{fl/fl}$ mice for conditional gene ablation in sensory neurons.

Funding sources:

The GSF facility has been constructed in part with the support from UT Health San Antonio, NIH/NCI P30 CA054174 (Cancer Center at UT Health San Antonio), NIGMS/NIH S10 Shared Instrumentation Grant Program (SIG) (S10OD021805-01 to Z.L.), and Cancer Prevention Research Institute of Texas (CPRIT) Core Facility Award (RP160732). This work was supported by NINDS/NIH NS102161 (to T.J.P and A.N.A.); NINDS/NIH NS104200 (to G.D and A.N.A.); NIH/NIGMS GM112747 (to A.N.A.); NINDS/NIH NS065926 (to T.J.P.); UT BRAIN Pilot Program ID: 1503083 (to G.D. and A.N.A.); and A.V.T. was supported by the Morrison Trust Foundation and the William and Ella Owens Medical Research Foundation.

Reference:

Adan N, Guzman-Morales J, Ledesma-Colunga MG, Perales-Canales SI, Quintanar-Stephano A, Lopez-Barrera F, Mendez I, Moreno-Carranza B, Triebel J, Binart N, Martinez de la Escalera G, Thebault S, Clapp C, 2013. Prolactin promotes cartilage survival and attenuates inflammation in inflammatory arthritis. J Clin Invest.

Agalave NM, Rudjito R, Farinotti AB, Khoonsari PE, Sandor K, Nomura Y, Szabo-Pardi TA, Urbina CM, Palada V, Price TJ, Erlandsson Harris H, Burton MD, Kultima K, Svensson CI, 2021. Sex-dependent role of microglia in disulfide high mobility group box 1 protein-mediated mechanical hypersensitivity. Pain 162, 446–458. [PubMed: 32773600]

Aitcheson SM, Frentiu FD, Hurn SE, Edwards K, Murray RZ, 2021. Skin Wound Healing: Normal Macrophage Function and Macrophage Dysfunction in Diabetic Wounds. Molecules 26.

Aley KO, Messing RO, Mochly-Rosen D, Levine JD, 2000. Chronic hypersensitivity for inflammatory nociceptor sensitization mediated by the epsilon isozyme of protein kinase C. Journal of Neuroscience 20, 4680–4685. [PubMed: 10844037]

Anders S, Huber W, 2010. Differential expression analysis for sequence count data. Genome Biol 11, R106. [PubMed: 20979621]

Anders S, Pyl PT, Huber W, 2015. HTSeq--a Python framework to work with high-throughput sequencing data. Bioinformatics 31, 166–169. [PubMed: 25260700]

Anderson GM, Beijer P, Bang AS, Fenwick MA, Bunn SJ, Grattan DR, 2006. Suppression of prolactin-induced signal transducer and activator of transcription 5b signaling and induction of suppressors of cytokine signaling messenger ribonucleic acid in the hypothalamic arcuate nucleus of the rat during late pregnancy and lactation. Endocrinology 147, 4996–5005. [PubMed: 16857756]

Avona A, Burgos-Vega C, Burton MD, Akopian A, Price TJ, Dussor G, 2019. Dural calcitonin gene-related peptide produces female-specific responses in rodent migraine models. J Neurosci.

Avona A, Mason BN, Burgos-Vega C, Hovhannisyan AH, Belugin SN, Mecklenburg J, Goffin V, Wajahat N, Price TJ, Akopian AN, Dussor G, 2021. Meningeal CGRP-Prolactin Interaction Evokes Female-Specific Migraine Behavior. Ann Neurol 89, 1129–1144. [PubMed: 33749851]

Basham B, Sathe M, Grein J, McClanahan T, D'Andrea A, Lees E, Rascle A, 2008. In vivo identification of novel STAT5 target genes. Nucleic Acids Res 36, 3802–3818. [PubMed: 18492722]

Belugin S, Diogenes AR, Patil MJ, Ginsburg E, Henry MA, Akopian AN, 2013. Mechanisms of Transient Signaling via Short and Long Prolactin Receptor Isoforms in Female and Male Sensory Neurons. J Biol Chem 288, 34943–34955. [PubMed: 24142695]

Ben-Jonathan N, LaPensee CR, LaPensee EW, 2008. What can we learn from rodents about prolactin in humans? Endocrine Reviews 29, 1–41. [PubMed: 18057139]

Berkley KJ, 1997. Sex differences in pain. Behav Brain Sci 20, 371–380; discussion 435–513. [PubMed: 10097000]

Berta T, Qadri YJ, Chen G, Ji RR, 2016. Microglial Signaling in Chronic Pain with a Special Focus on Caspase 6, p38 MAP Kinase, and Sex Dependence. J Dent Res 95, 1124–1131. [PubMed: 27307048]

Bole-Feysot C, Goffin V, Edery M, Binart N, Kelly PA, 1998a. Prolactin (PRL) and its receptor: actions, signal transduction pathways and phenotypes observed in PRL receptor knockout mice. Endocr Rev 19, 225–268. [PubMed: 9626554]

Bole-Feysot C, Goffin V, Edery M, Binart N, Kelly PA, 1998b. Prolactin (PRL) and its receptor: actions, signal transduction pathways and phenotypes observed in PRL receptor knockout mice. Endocrine Reviews 19, 225–268. [PubMed: 9626554]

Borba VV, Zandman-Goddard G, Shoenfeld Y, 2019. Prolactin and autoimmunity: The hormone as an inflammatory cytokine. Best Pract Res Clin Endocrinol Metab, 101324. [PubMed: 31564625]

Brand JM, Frohn C, Cziupka K, Brockmann C, Kirchner H, Luhm J, 2004. Prolactin triggers pro-inflammatory immune responses in peripheral immune cells. Eur Cytokine Netw 15, 99–104. [PubMed: 15319167]

Brown RS, Kokay IC, Phillipps HR, Yip SH, Gustafson P, Wyatt A, Larsen CM, Knowles P, Ladyman SR, LeTissier P, Grattan DR, 2016. Conditional Deletion of the Prolactin Receptor Reveals Functional Subpopulations of Dopamine Neurons in the Arcuate Nucleus of the Hypothalamus. J Neurosci 36, 9173–9185. [PubMed: 27581458]

Brown RSE, Aoki M, Ladyman SR, Phillipps HR, Wyatt A, Boehm U, Grattan DR, 2017. Prolactin action in the medial preoptic area is necessary for postpartum maternal nursing behavior. Proc Natl Acad Sci U S A 114, 10779–10784. [PubMed: 28923971]

Cabrera-Reyes EA, Vanoye-Carlo A, Rodriguez-Dorantes M, Vazquez-Martinez ER, Rivero-Segura NA, Collazo-Navarrete O, Cerbon M, 2019. Transcriptomic analysis reveals new hippocampal gene networks induced by prolactin. Sci Rep 9, 13765. [PubMed: 31551509]

Candlish M, De Angelis R, Gotz V, Boehm U, 2015. Gene Targeting in Neuroendocrinology. Compr Physiol 5, 1645–1676. [PubMed: 26426463]

Carreno PC, Jimenez E, Sacedon R, Vicente A, Zapata AG, 2004. Prolactin stimulates maturation and function of rat thymic dendritic cells. J Neuroimmunol 153, 83–90. [PubMed: 15265666]

Chaplan SR, Bach FW, Pogrel JW, Chung JM, Yaksh TL, 1994. Quantitative assessment of tactile allodynia in the rat paw. J Neurosci Methods 53, 55–63. [PubMed: 7990513]

Chen G, Zhang YQ, Qadri YJ, Serhan CN, Ji RR, 2018. Microglia in Pain: Detrimental and Protective Roles in Pathogenesis and Resolution of Pain. Neuron 100, 1292–1311. [PubMed: 30571942]

Chen Y, Moutal A, Navratilova E, Kopruszinski C, Yue X, Ikegami M, Chow M, Kanazawa I, Bellampalli SS, Xie J, Patwardhan A, Rice K, Fields H, Akopian A, Neugebauer V, Dodick D,

Khanna R, Porreca F, 2020. The prolactin receptor long isoform regulates nociceptor sensitization and opioid-induced hyperalgesia selectively in females. Sci Transl Med 12.

Chow LH, Chen YH, Lai CF, Lin TY, Chen YJ, Kao JH, Huang EY, 2018. Sex Difference of Angiotensin IV-, LVV-Hemorphin 7-, and Oxytocin-Induced Antiallodynia at the Spinal Level in Mice With Neuropathic Pain. Anesth Analg 126, 2093–2101. [PubMed: 29381512]

De Bellis A, Bizzarro A, Pivonello R, Lombardi G, Bellastella A, 2005. Prolactin and autoimmunity. Pituitary 8, 25–30. [PubMed: 16411065]

Dimitrov S, Lange T, Fehm HL, Born J, 2004. A regulatory role of prolactin, growth hormone, and corticosteroids for human T-cell production of cytokines. Brain Behav Immun 18, 368–374. [PubMed: 15157954]

Diogenes A, Patwardhan AM, Jeske NA, Ruparel NB, Goffin V, Akopian AN, Hargreaves KM, 2006. Prolactin modulates TRPV1 in female rat trigeminal sensory neurons. Journal of Neuroscience 26, 8126–8136. [PubMed: 16885226]

Dominguez-Andres J, Joosten LA, Netea MG, 2019. Induction of innate immune memory: the role of cellular metabolism. Curr Opin Immunol 56, 10–16. [PubMed: 30240964]

Durante M, Squillace S, Lauro F, Giancotti LA, Coppi E, Cherchi F, Di Cesare Mannelli L, Ghelardini C, Kolar G, Wahlman C, Opejin A, Xiao C, Reitman ML, Tosh DK, Hawiger D, Jacobson KA, Salvemini D, 2021. Adenosine A3 agonists reverse neuropathic pain via T cell-mediated production of IL-10. J Clin Invest 131.

Eijkelkamp N, Steen-Louws C, Hartgring SA, Willemen HL, Prado J, Lafeber FP, Heijnen CJ, Hack CE, van Roon JA, Kavelaars A, 2016. IL4–10 Fusion Protein Is a Novel Drug to Treat Persistent Inflammatory Pain. J Neurosci 36, 7353–7363. [PubMed: 27413147]

Fillingim RB, Bruehl S, Dworkin RH, Dworkin SF, Loeser JD, Turk DC, Widerstrom-Noga E, Arnold L, Bennett R, Edwards RR, Freeman R, Gewandter J, Hertz S, Hochberg M, Krane E, Mantyh PW, Markman J, Neogi T, Ohrbach R, Paice JA, Porreca F, Rappaport BA, Smith SM, Smith TJ, Sullivan MD, Verne GN, Wasan AD, Wesselmann U, 2014. The ACTTION-American Pain Society Pain Taxonomy (AAPT): An Evidence-Based and Multidimensional Approach to Classifying Chronic Pain Conditions. J Pain 15, 241–249. [PubMed: 24581634]

Fillingim RB, King CD, Ribeiro-Dasilva MC, Rahim-Williams B, Riley JL, 2009. Sex, Gender, and Pain: A Review of Recent Clinical and Experimental Findings. J Pain 10, 447–485. [PubMed: 19411059]

Freeman ME, Kanyicska B, Lerant A, Nagy G, 2000. Prolactin: structure, function, and regulation of secretion. Physiological Reviews 80, 1523–1631. [PubMed: 11015620]

Ghasemlou N, Chiu IM, Julien JP, Woolf CJ, 2015. CD11b+Ly6G- myeloid cells mediate mechanical inflammatory pain hypersensitivity. Proc Natl Acad Sci U S A 112, E6808–6817. [PubMed: 26598697]

Ji RR, Xu ZZ, Strichartz G, Serhan CN, 2011. Emerging roles of resolvins in the resolution of inflammation and pain. Trends Neurosci 34, 599–609. [PubMed: 21963090]

Joseph EK, Parada CA, Levine JD, 2003. Hyperalgesic priming in the rat demonstrates marked sexual dimorphism. Pain 105, 143–150. [PubMed: 14499430]

Kanai T, Seki S, Jenks JA, Kohli A, Kawli T, Martin DP, Snyder M, Bacchetta R, Nadeau KC, 2014. Identification of STAT5A and STAT5B target genes in human T cells. PLoS One 9, e86790. [PubMed: 24497979]

Kelly PA, Djiane J, Postel-Vinay MC, Edery M, 1991. The prolactin/growth hormone receptor family. Endocrine Reviews 12, 235–251. [PubMed: 1935820]

Khomula EV, Ferrari LF, Araldi D, Levine JD, 2017. Sexual Dimorphism in a Reciprocal Interaction of Ryanodine and IP3 Receptors in the Induction of Hyperalgesic Priming. J Neurosci 37, 2032–2044. [PubMed: 28115480]

Krukowski K, Eijkelkamp N, Laumet G, Hack CE, Li Y, Dougherty PM, Heijnen CJ, Kavelaars A, 2016. CD8+ T Cells and Endogenous IL-10 Are Required for Resolution of Chemotherapy-Induced Neuropathic Pain. J Neurosci 36, 11074–11083. [PubMed: 27798187]

Lampert MA, Gustafsson AB, 2019. Mitochondria and autophagy in adult stem cells: proliferate or differentiate. J Muscle Res Cell Motil.

Laumet G, Edralin JD, Dantzer R, Heijnen CJ, Kavelaars A, 2019. Cisplatin educates CD8+ T cells to prevent and resolve chemotherapy-induced peripheral neuropathy in mice. Pain 160, 1459–1468. [PubMed: 30720585]

Liu CM, Davis EA, Suarez AN, Wood RI, Noble EE, Kanoski SE, 2020. Sex Differences and Estrous Influences on Oxytocin Control of Food Intake. Neuroscience 447, 63–73. [PubMed: 31738883]

Luo X, Chen O, Wang Z, Bang S, Ji J, Lee SH, Huh Y, Furutani K, He Q, Tao X, Ko MC, Bortsov A, Donnelly CR, Chen Y, Nackley A, Berta T, Ji RR, 2021. IL-23/IL-17A/TRPV1 axis produces mechanical pain via macrophage-sensory neuron crosstalk in female mice. Neuron 109, 2691–2706 e2695. [PubMed: 34473953]

Marano RJ, Ben-Jonathan N, 2014. Minireview: Extrapituitary Prolactin: An Update on the Distribution, Regulation, and Functions. Molecular Endocrinology 28, 622–633. [PubMed: 24694306]

Mecklenburg J, Zou Y, Wangzhou A, Garcia D, Lai Z, Tumanov AV, Dussor G, Price TJ, Akopian AN, 2020. Transcriptomic sex differences in sensory neuronal populations of mice. Sci Rep 10, 15278. [PubMed: 32943709]

Melemedjian OK, Asiedu MN, Tillu DV, Peebles KA, Yan J, Ertz N, Dussor GO, Price TJ, 2010. IL-6- and NGF-induced rapid control of protein synthesis and nociceptive plasticity via convergent signaling to the eIF4F complex. J Neurosci 30, 15113–15123. [PubMed: 21068317]

Mogil JS, 2020. Qualitative sex differences in pain processing: emerging evidence of a biased literature. Nat Rev Neurosci 21, 353–365. [PubMed: 32440016]

Mogil JS, Wilson SG, Chesler EJ, Rankin AL, Nemmani KV, Lariviere WR, Groce MK, Wallace MR, Kaplan L, Staud R, Ness TJ, Glover TL, Stankova M, Mayorov A, Hruby VJ, Grisel JE, Fillingim RB, 2003. The melanocortin-1 receptor gene mediates female-specific mechanisms of analgesia in mice and humans. Proc Natl Acad Sci U S A 100, 4867–4872. [PubMed: 12663858]

Paige C, Barba-Escobedo PA, Mecklenburg J, Patil M, Goffin V, Grattan DR, Dussor G, Akopian AN, Price TJ, 2020. Neuroendocrine Mechanisms Governing Sex Differences in Hyperalgesic Priming Involve Prolactin Receptor Sensory Neuron Signaling. J Neurosci 40, 7080–7090. [PubMed: 32801151]

Paige C, Maruthy GB, Mejia G, Dussor G, Price T, 2018. Spinal Inhibition of P2XR or p38 Signaling Disrupts Hyperalgesic Priming in Male, but not Female, Mice. Neuroscience 385, 133–142. [PubMed: 29913243]

Patil M, Belugin S, Mecklenburg J, Wangzhou A, Paige C, Barba-Escobedo PA, Boyd JT, Goffin V, Grattan D, Boehm U, Dussor G, Price TJ, Akopian AN, 2019a. Prolactin Regulates Pain Responses via a Female-Selective Nociceptor-Specific Mechanism. iScience 20, 449–465. [PubMed: 31627131]

Patil M, Hovhannisyan AH, Wangzhou A, Mecklenburg J, Koek W, Goffin V, Grattan D, Boehm U, Dussor G, Price TJ, Akopian AN, 2019b. Prolactin receptor expression in mouse dorsal root ganglia neuronal subtypes is sex-dependent. J Neuroendocrinol 31, e12759. [PubMed: 31231869]

Patil MJ, Henry MA, Akopian AN, 2014. Prolactin receptor in regulation of neuronal excitability and channels. Channels (Austin) 8, 193–202. [PubMed: 24758841]

Patil MJ, Ruparel SB, Henry MA, Akopian AN, 2013. Prolactin regulates TRPV1, TRPA1, and TRPM8 in sensory neurons in a sex-dependent manner: Contribution of prolactin receptor to inflammatory pain. American journal of physiology. Endocrinology and metabolism 305, E1154–1164. [PubMed: 24022869]

Price TJ, Basbaum AI, Bresnahan J, Chambers JF, De Koninck Y, Edwards RR, Ji RR, Katz J, Kavelaars A, Levine JD, Porter L, Schechter N, Sluka KA, Terman GW, Wager TD, Yaksh TL, Dworkin RH, 2018. Transition to chronic pain: opportunities for novel therapeutics. Nat Rev Neurosci 19, 383–384. [PubMed: 29765159]

Price TJ, Ray PR, 2019. Recent advances toward understanding the mysteries of the acute to chronic pain transition. Curr Opin Physiol 11, 42–50. [PubMed: 32322780]

Rani A, Murphy JJ, 2016. STAT5 in Cancer and Immunity. J Interferon Cytokine Res 36, 226–237. [PubMed: 26716518]

Rosen SF, Ham B, Drouin S, Boachie N, Chabot-Dore AJ, Austin JS, Diatchenko L, Mogil JS, 2017. T-Cell Mediation of Pregnancy Analgesia Affecting Chronic Pain in Mice. J Neurosci 37, 9819–9827. [PubMed: 28877966]

Rudjito R, Agalave NM, Farinotti AB, Lundback P, Szabo-Pardi TA, Price TJ, Harris HE, Burton MD, Svensson CI, 2021. Sex- and cell-dependent contribution of peripheral high mobility group box 1 and TLR4 in arthritis-induced pain. Pain 162, 459–470. [PubMed: 32796317]

Sanford LM, Baker SJ, 2010. Prolactin regulation of testosterone secretion and testes growth in DLS rams at the onset of seasonal testicular recrudescence. Reproduction 139, 197–207. [PubMed: 19755483]

Scotland PE, Patil M, Belugin S, Henry MA, Goffin V, Hargreaves KM, Akopian AN, 2011. Endogenous prolactin generated during peripheral inflammation contributes to thermal hyperalgesia. Eur J Neurosci 34, 745–754. [PubMed: 21777304]

Sommer C, Leinders M, Uceyler N, 2018. Inflammation in the pathophysiology of neuropathic pain. Pain 159, 595–602. [PubMed: 29447138]

Sorge RE, LaCroix-Fralish ML, Tuttle AH, Sotocinal SG, Austin JS, Ritchie J, Chanda ML, Graham AC, Topham L, Beggs S, Salter MW, Mogil JS, 2011. Spinal cord Toll-like receptor 4 mediates inflammatory and neuropathic hypersensitivity in male but not female mice. J Neurosci 31, 15450–15454. [PubMed: 22031891]

Sorge RE, Mapplebeck JC, Rosen S, Beggs S, Taves S, Alexander JK, Martin LJ, Austin JS, Sotocinal SG, Chen D, Yang M, Shi XQ, Huang H, Pillon NJ, Bilan PJ, Tu Y, Klip A, Ji RR, Zhang J, Salter MW, Mogil JS, 2015. Different immune cells mediate mechanical pain hypersensitivity in male and female mice. Nat Neurosci 18, 1081–1083. [PubMed: 26120961]

Staff NP, Fehrenbacher JC, Caillaud M, Damaj MI, Segal RA, Rieger S, 2019. Pathogenesis of paclitaxel-induced peripheral neuropathy: A current review of in vitro and in vivo findings using rodent and human model systems. Exp Neurol 324, 113121. [PubMed: 31758983]

Stirling LC, Forlani G, Baker MD, Wood JN, Matthews EA, Dickenson AH, Nassar MA, 2005. Nociceptor-specific gene deletion using heterozygous NaV1.8-Cre recombinase mice. Pain 113, 27–36. [PubMed: 15621361]

Teglund S, McKay C, Schuetz E, van Deursen JM, Stravopodis D, Wang D, Brown M, Bodner S, Grosveld G, Ihle JN, 1998. Stat5a and Stat5b proteins have essential and nonessential, or redundant, roles in cytokine responses. Cell 93, 841–850. [PubMed: 9630227]

Trapnell C, Pachter L, Salzberg SL, 2009. TopHat: discovering splice junctions with RNA-Seq. Bioinformatics 25, 1105–1111. [PubMed: 19289445]

Trapnell C, Roberts A, Goff L, Pertea G, Kim D, Kelley DR, Pimentel H, Salzberg SL, Rinn JL, Pachter L, 2012. Differential gene and transcript expression analysis of RNA-seq experiments with TopHat and Cufflinks. Nat Protoc 7, 562–578. [PubMed: 22383036]

Traub RJ, Ji Y, 2013. Sex differences and hormonal modulation of deep tissue pain. Front Neuroendocrinol 34, 350–366. [PubMed: 23872333]

Unruh AM, 1996. Gender variations in clinical pain experience. Pain 65, 123–167. [PubMed: 8826503]

Utama FE, LeBaron MJ, Neilson LM, Sultan AS, Parlow AF, Wagner KU, Rui H, 2006. Human prolactin receptors are insensitive to mouse prolactin: implications for xenotransplant modeling of human breast cancer in mice. J Endocrinol 188, 589–601. [PubMed: 16522738]

Utama FE, Tran TH, Ryder A, LeBaron MJ, Parlow AF, Rui H, 2009. Insensitivity of human prolactin receptors to nonhuman prolactins: relevance for experimental modeling of prolactin receptor-expressing human cells. Endocrinology 150, 1782–1790. [PubMed: 19022890]

Wang X, Chen J, Xu J, Xie J, Harris DCH, Zheng G, 2021. The Role of Macrophages in Kidney Fibrosis. Front Physiol 12, 705838. [PubMed: 34421643]

Willemen HL, Eijkelkamp N, Garza Carbajal A, Wang H, Mack M, Zijlstra J, Heijnen CJ, Kavelaars A, 2014. Monocytes/Macrophages control resolution of transient inflammatory pain. J Pain 15, 496–506. [PubMed: 24793056]

Woolf CJ, 2011. Central sensitization: implications for the diagnosis and treatment of pain. Pain 152, S2–S15. [PubMed: 20961685]

Xie W, Strong JA, Zhang JM, 2017. Active Nerve Regeneration with Failed Target Reinnervation Drives Persistent Neuropathic Pain. eNeuro 4.

Yu X, Liu H, Hamel KA, Morvan MG, Yu S, Leff J, Guan Z, Braz JM, Basbaum AI, 2020. Dorsal root ganglion macrophages contribute to both the initiation and persistence of neuropathic pain. Nat Commun 11, 264. [PubMed: 31937758]

Yu YR, O'Koren EG, Hotten DF, Kan MJ, Kopin D, Nelson ER, Que L, Gunn MD, 2016. A Protocol for the Comprehensive Flow Cytometric Analysis of Immune Cells in Normal and Inflamed Murine Non-Lymphoid Tissues. PLoS One 11, e0150606. [PubMed: 26938654]

Highlights:

- Prolactin treatment generates sex-differences in pain trajectories in mice
- Low dose prolactin treatment causes a non-resolving pain phenotype in females
- Pain resolution is preceded by pro-inflammatory $CD11b^{+}/CD64^{+}$ cell responses
- Female non-resolving pain linked to tissue damage without an inflammatory response

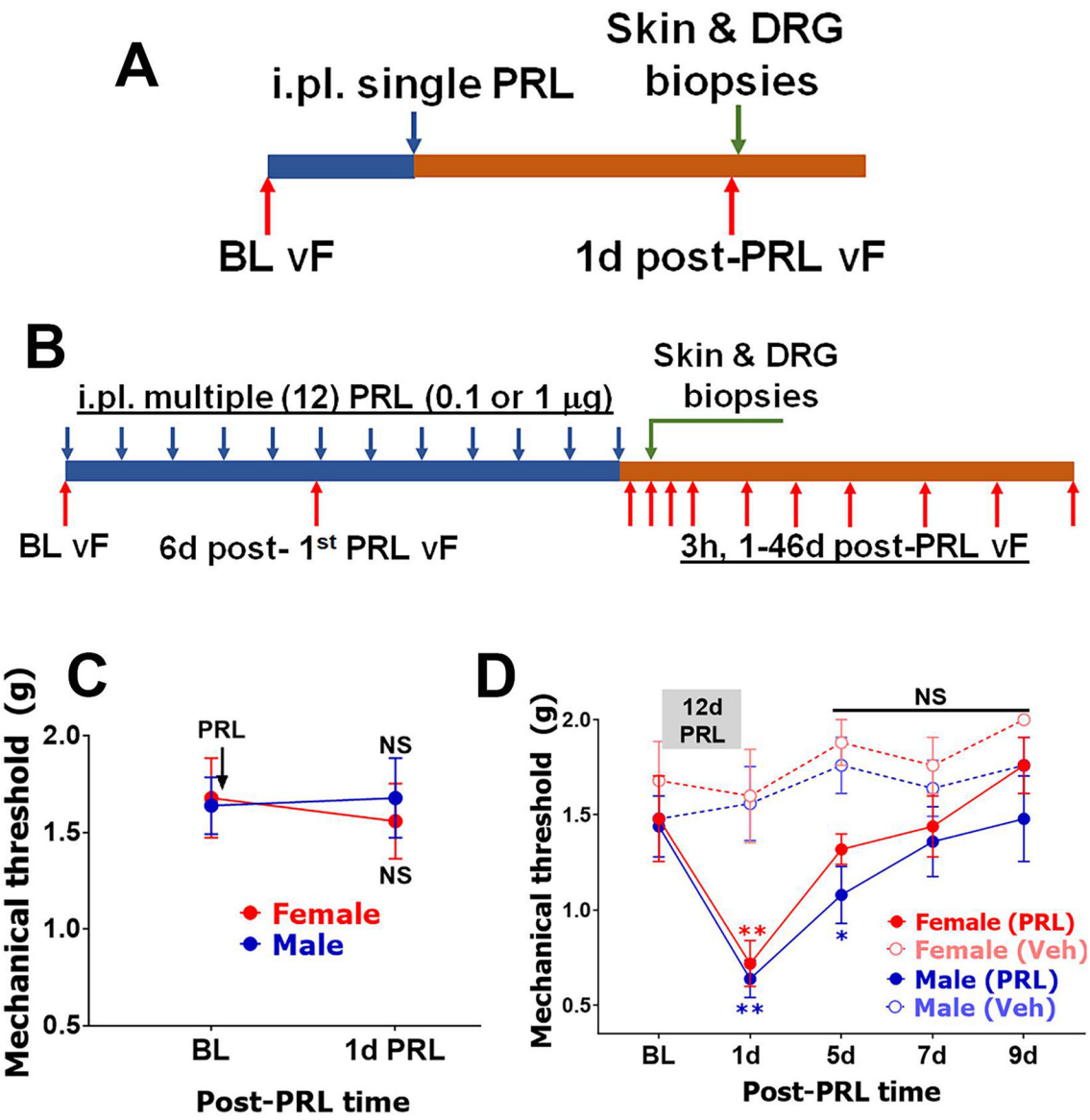

Figure 1: Single and multiple intra-plantar (i.pl.) injection 1µg PRL-induced mechanical hypersensitivity

A: Schematic of experiments with single i.pl. injection of PRL (0.1 or 1µg) marked with blue arrow. **B:** Schematic of experiments with multiple (12 daily) consecutive i.pl. injections of PRL (0.1 or 1µg) marked with blue arrows. Red arrows show time points for measurement of baseline (BL) and post-PRL mechanical hypersensitivity with von Frey filaments (vF). Green arrows show time point for sample collections. **C**: BL mechanical responses were assessed, and then single PRL (1µg) i.pl. injection was carried out. One day post-PRL injection mechanical threshold responses were measured in ipsilateral hind paws of female and male mice. **D**: After BL measurement, PRL (1µg) or vehicle (Veh) was i.pl. injected once per day for 12d in females and males. At 1d post-last PRL or Veh injection, mechanical threshold responses were measured in ipsilateral hind paws of female and male mice. Statistical analysis is 2-way ANOVA with Bonferroni's post-hoc test (NS – non-significant; * $p<0.05$; ** $p<0.01$; n=5–7).

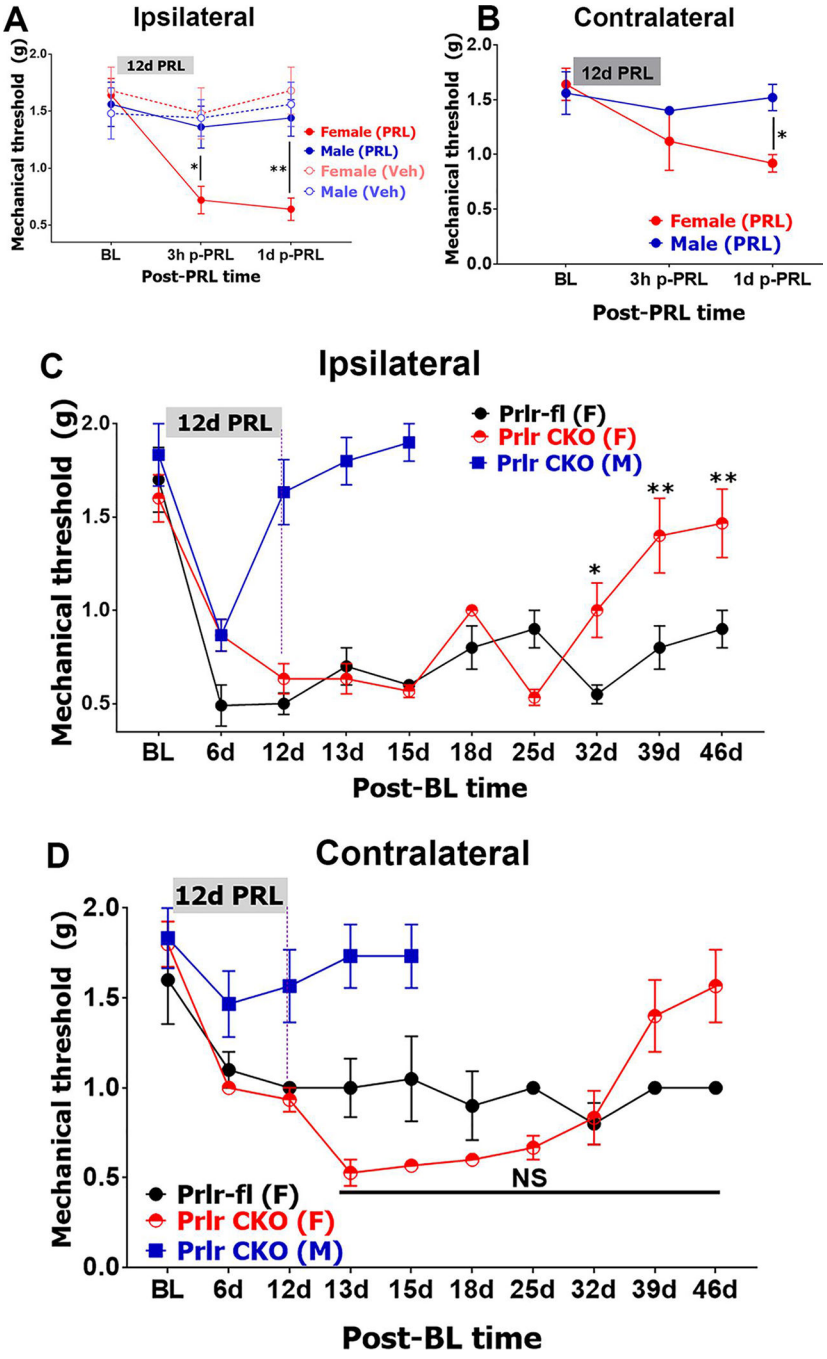

Figure 2: Multiple i.pl. injection 0.1μg PRL-induced sex-dependent mechanical hypersensitivity

A, B: After BL measurement, PRL (0.1μg) or vehicle (Veh) was i.pl. injected once per day for 12d in females and males. At 3h and 1d post-last PRL (pPRL) or Veh injection, mechanical threshold responses were measured in ipsilateral (*panel A*) or contralateral (*panel B*) hind paws of female and male mice. **C, D**: After BL measurement, PRL (0.1μg) was i.pl. injected once per day for 12d in $Prlr^{fl/fl}$ (control) and $Nav1.8^{cre/-}/Prlr^{fl/fl}$ (Prlr CKO) females and males. Mechanical threshold responses were assessed in ipsilateral (*panel C*) or contralateral (*panel D*) hind paws at indicated time points counted from post-first PRL

injection. Twelve-day long PRL application is marked by gray bar on all panels. Statistic is 2-way ANOVA with Bonferroni's post-hoc test, compare cell means regardless of rows and columns (NS – non-significant; * $p<0.05$; ** $p<0.01$ n=5–7).

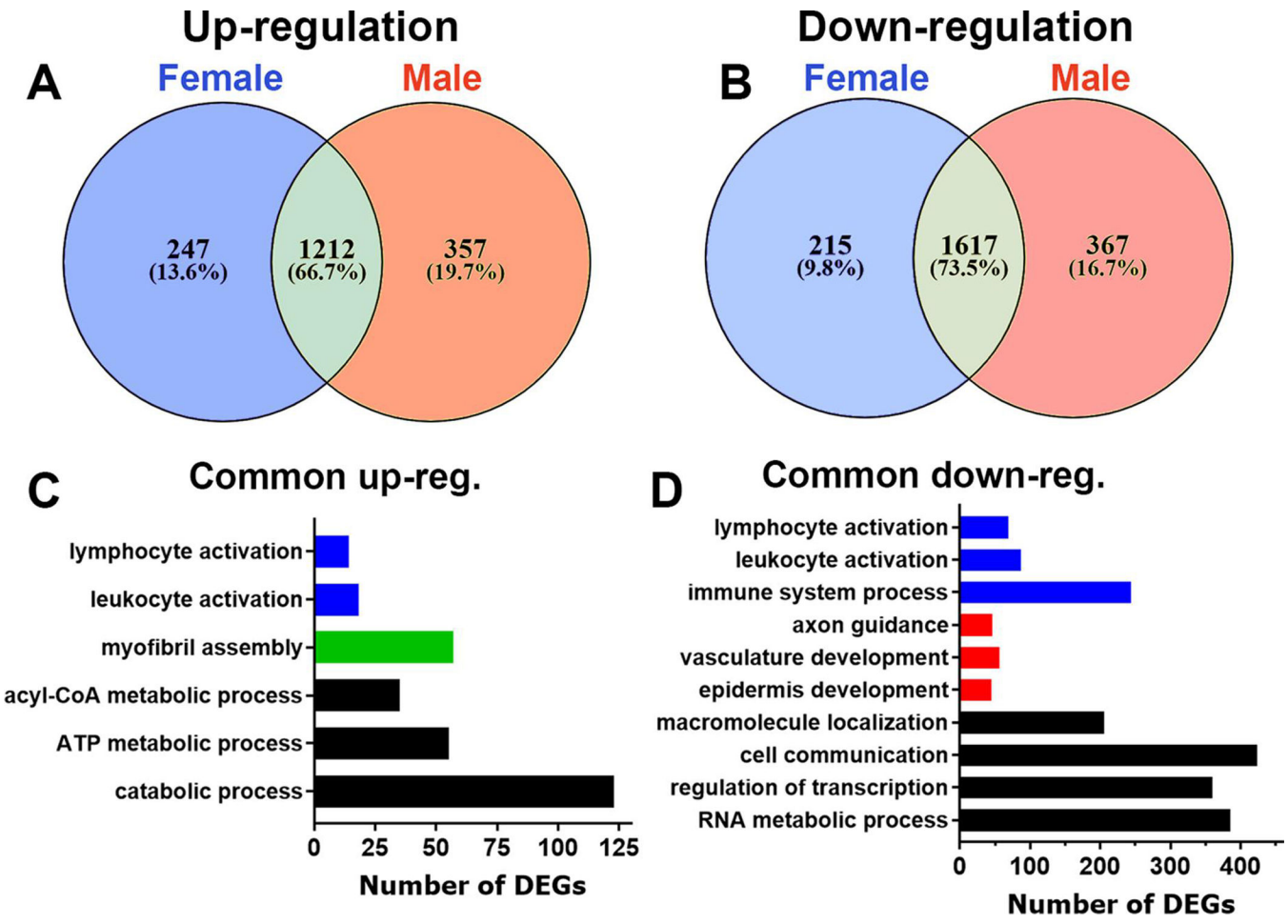

Figure 3: Gene regulation in hind paw skin at 1d post-single i.pl. PRL injection

A, B: Venn diagram of up-regulated (*panel A*) and down-regulated (*panel B*) genes in hind paw skin of females and males at 1d post-single i.pl. injection of PRL (1μg). Numbers and relative percentages of female-selective, male-selective, and common (for males and females) genes are indicated. **C, D**: Biological processes for up-regulated (*panel C*) and down-regulated (*panel D*) common genes at 1d post-single i.pl. injection of PRL (1μg). X-axis on *the panels C* and *D* represents numbers of deferentially regulated genes (DEGs). Y-axis notes biological processes.

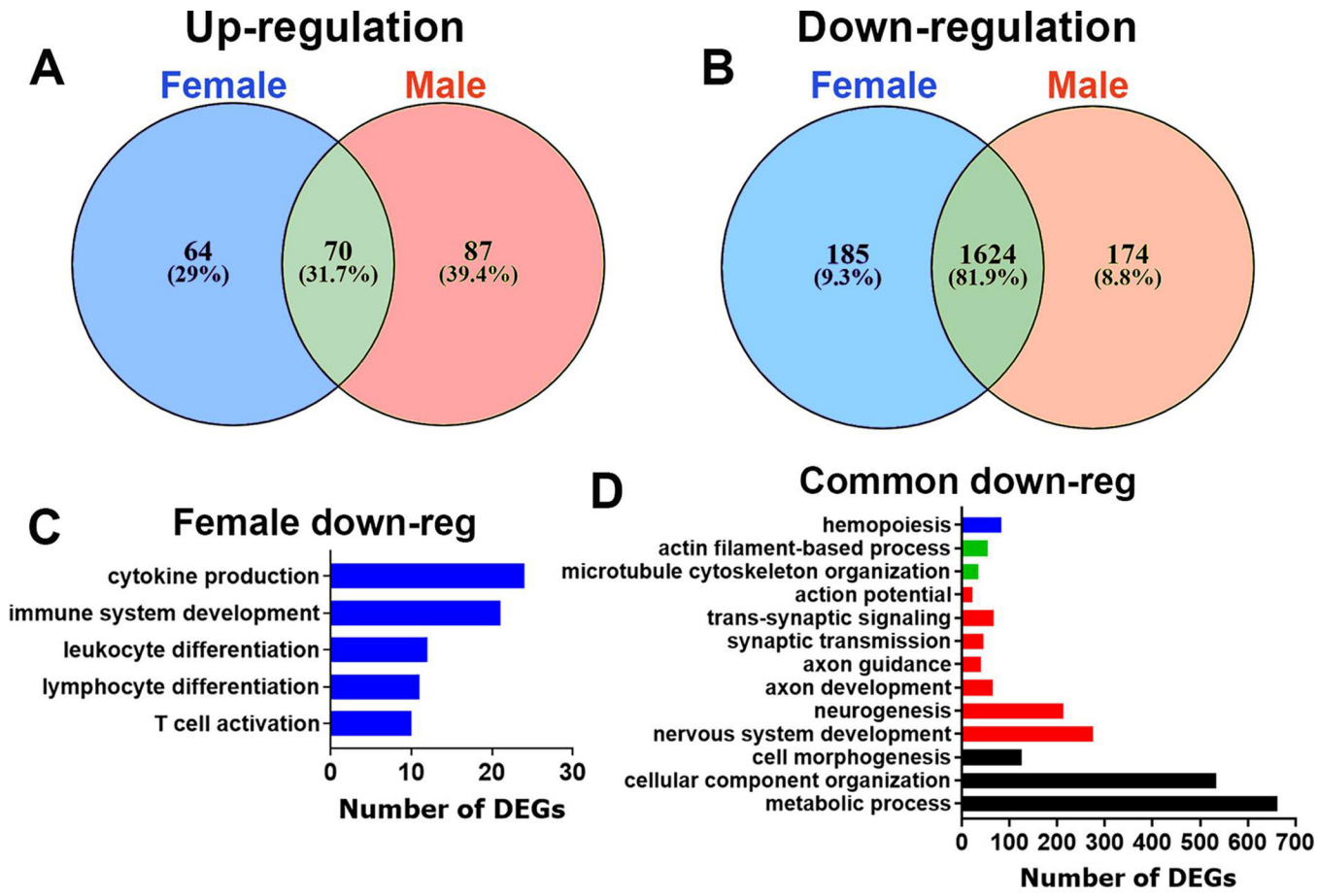

Figure 4: Gene regulation in DRG at 1d post-single i.pl. PRL injection

A, B: Venn diagram of up-regulated (*panel A*) and down-regulated (*panel B*) genes in DRG of females and males at 1d post-single i.pl. injection of PRL (1μg). Numbers and relative percentages of female-selective, male-selective, and common genes are indicated. **C, D**: Biological processes for female-selective down-regulated (*panel C*) and common down-regulated (*panel D*) genes at 1d post-single i.pl. injection of PRL (1μg). X-axis on *the panels C* and *D* represents numbers of DEGs. Y-axis notes biological processes.

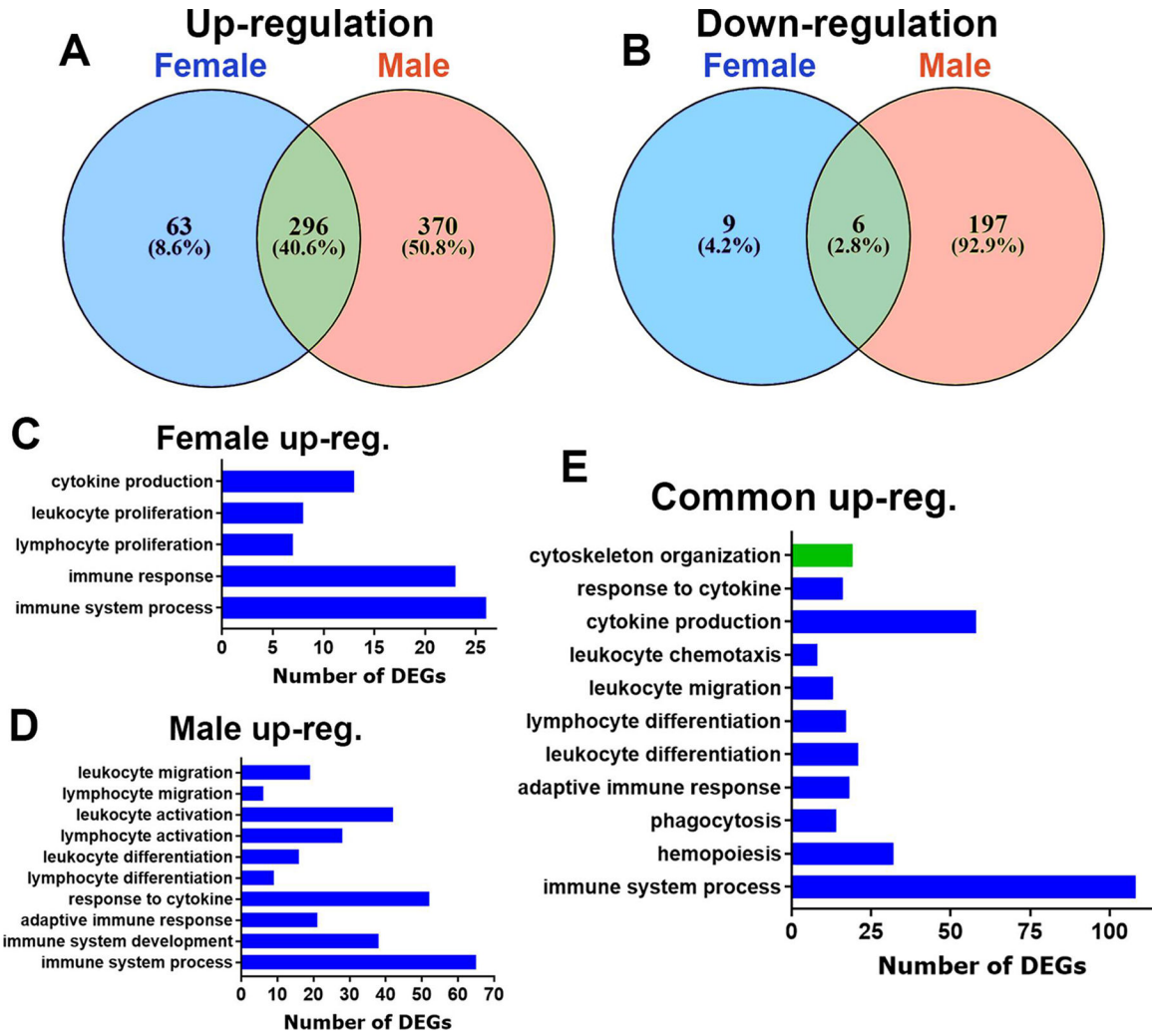

Figure 5: Gene regulation in hind paw skin at 1d post 12-days-long i.pl. 1μg PRL injections

A, B: Venn diagram of up-regulated (*panel A*) and down-regulated (*panel B*) genes in hind paw skin of females and males at 1d after 12 consecutive daily i.pl. injection of PRL (1μg). Numbers and relative percentages of female-selective, male-selective, and common (for males and females) genes are indicated. **C-E**: Biological processes for up-regulated female-selective (*panel C*), male-selective (*panel D*) and common (*panel E*) genes at 1d after 12 consecutive daily i.pl. injection of PRL (1μg). X-axis on *the panels C-E* represents numbers of DEGs. Y-axis notes biological processes.

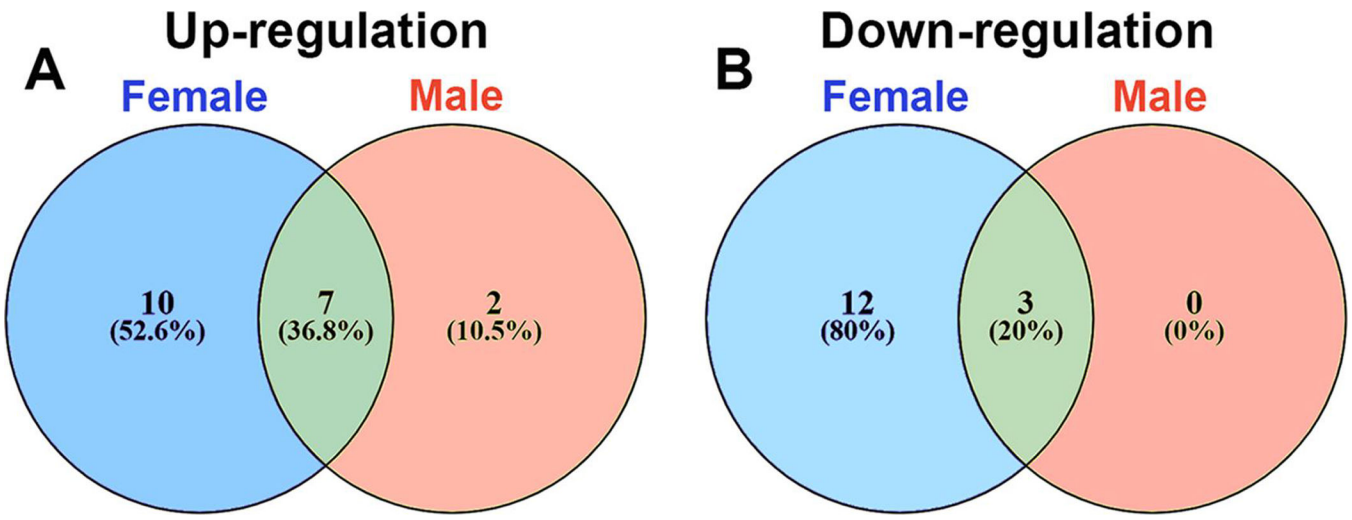

Figure 6: Gene regulation in DRG at 1d post 12-days-long i.pl. 1μg PRL injections

A, B: Venn diagram of up-regulated (*panel A*) and down-regulated (*panel B*) genes in DRG of females and males at 1d after 12 consecutive daily i.pl. injection of PRL (1μg). Numbers and relative percentages of female-selective, male-selective, and common genes are indicated.

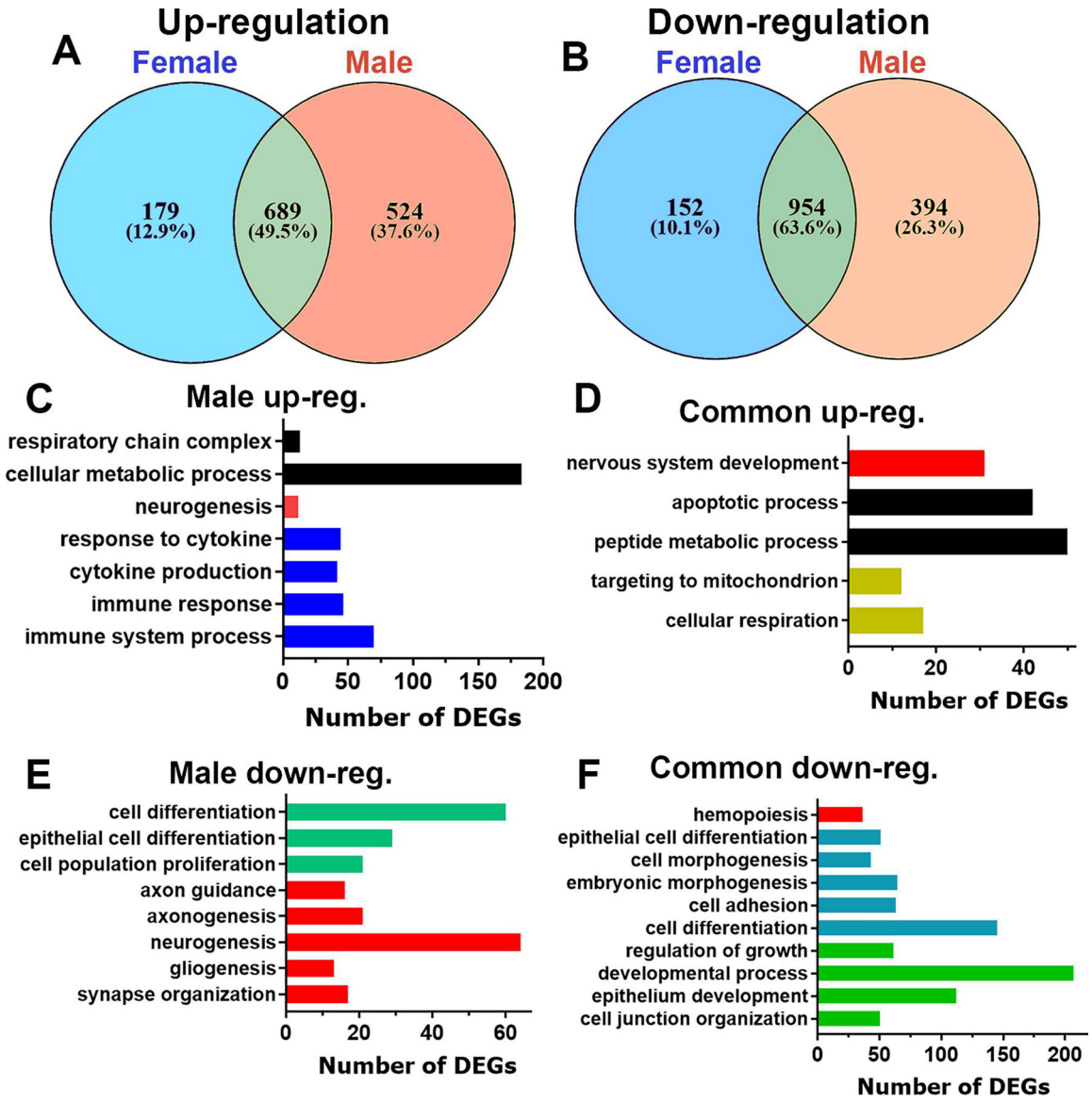

Figure 7: Gene regulation in hind paw skin at 1d post 12-days-long i.pl. 0.1μg PRL injections

A, B: Venn diagram of up-regulated (*panel A*) and down-regulated (*panel B*) genes at 1d after 12 consecutive daily i.pl. injection of PRL (0.1μg). Numbers and relative percentages of female-selective, male-selective, and common genes are indicated. **C-F**: Biological processes for up-regulated male-selective (*panel C*) and common (*panel D*), as well as down-regulated male-selective (*panel E*) and common (*panel F*) genes at 1d after 12 consecutive daily i.pl. injection of PRL (0.1μg). X-axis on *the panels C-F* represents numbers of DEGs. Y-axis notes biological processes.

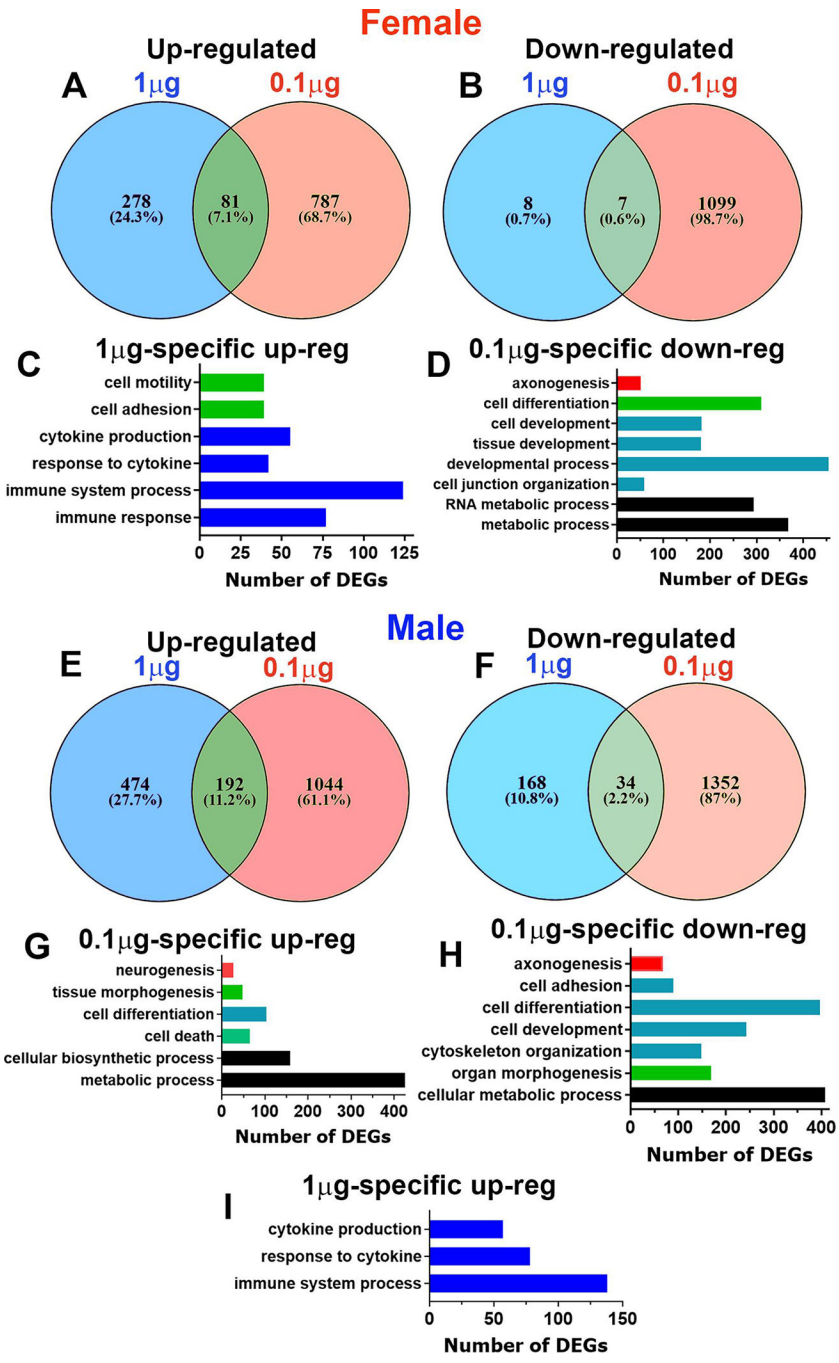

Figure 8: Comparisons of DEGs in female and male hind paws in 1μg and 0.1μg PRL multi-day treatments

A, B: Venn diagram of up-regulated (*panel A*) and down-regulated (*panel B*) female hind paw DEGs at 1d post-last PRL time point for multi-day 1μg and 0.1μg PRL i.pl. treatment models. Numbers and relative percentages of 1μg PRL model (1μg)-selective, 0.1μg PRL model (0.1μg)-selective and common for both models' genes are indicated. **C, D**: Biological processes for up-regulated 1μg PRL model-selective (*panel C*) and down-regulated 0.1μg PRL model-selective (*panel D*) genes in female hind paws. X-axis on *the panels C and*

D represents numbers of DEGs. Y-axis notes biological processes. **E, F**: Venn diagram of up-regulated (*panel A*) and down-regulated (*panel B*) male hind paw DEGs at 1d post-last PRL time point for multi-day 1μg and 0.1μg PRL i.pl. treatment models. Numbers and relative percentages of 1μg PRL (1μg)-selective, 0.1μg PRL (0.1μg)-selective and common for both models' genes are indicated. **G-I**: Biological processes for up-regulated (*panel G*) and down-regulated (*panel H*) 0.1μg PRL model-selective (*panel C*) and up-regulated 1μg PRL model-selective (*panel I*) genes. X-axis on *the panels G-I* represents numbers of DEGs. Y-axis notes biological processes.

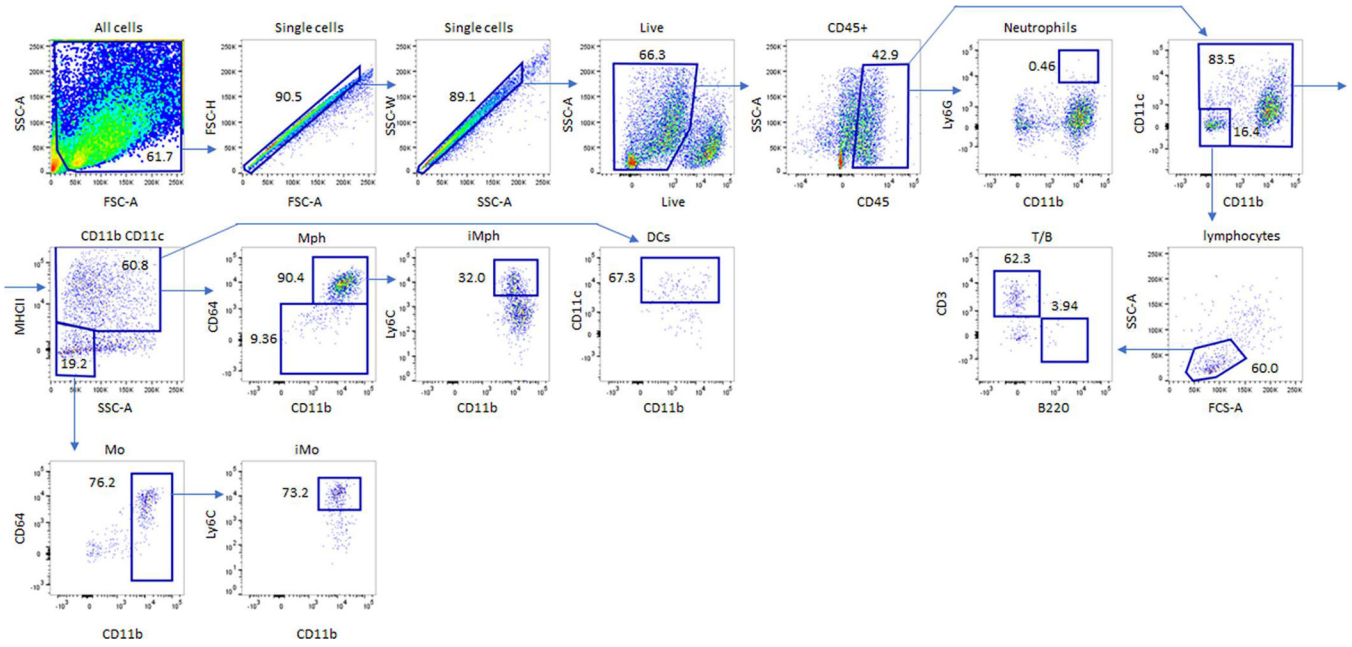

Figure 9: Gating strategy for flow cytometry

Gating strategy for single cell suspension from female paw treated by vehicle, single or multiple injections of PRL. The strategy shows how live singlets and then different immune cells were gated from single-cell suspension. Abbreviations are SSC-A - side angle scattered area; FSC-A - forward angle scattered area; MHCII – major histocompatibility complex class II; Mph – macrophages, iMph – inflammatory macrophages, Mo - monocytes, iMo – inflammatory monocytes, DCs – dendritic cells, T/B – T and B-cells

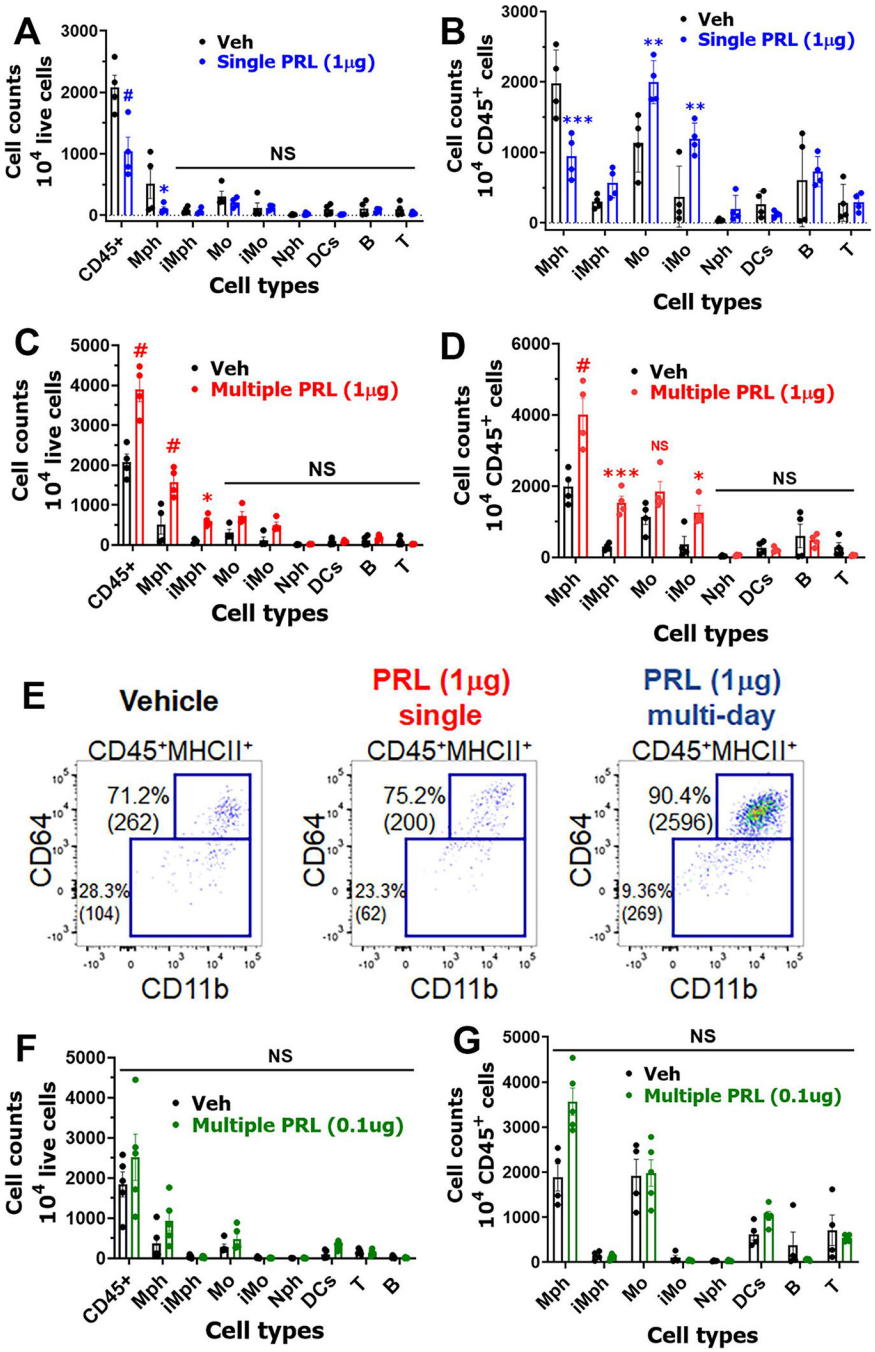

Fig. 10. Immune cell profiles in single and multiple i.pl. PRL treated female skin

A, B: Immune cell counts per 10^4 live cells (*panel A*) and per 10^4 $CD45^+$ cells (*panel B*) in female skin at 1d post-vehicle (Veh) or PRL (1 μg). PRL treatment single i.pl. **C, D**: Immune cell counts per 10^4 live cells (*panel C*) and per 10^4 $CD45^+$ cells (*panel D*) in hindpaw skin at 1d post-vehicle (Veh) or PRL (1 μg) i.pl. treatment for 12 consecutive days. **E:** Representative plots of $CD11b^+/CD64^+/MHCII^+$ macrophages from cell suspension of female paw i.pl. injected with Veh, single or multiple PRL (1 μg). **F, G:** Immune cell counts per 10^4 live cells (*panel F*) and per 10^4 $CD45^+$ cells (*panel G*) in female skin

at 1d post-vehicle (Veh) or PRL (0.1 μg) i.pl. treatment for 12 consecutive days. $CD45^+$ cells - all hematopoietic immune cells; DCs – dendritic cells; Mph – macrophages; iMph - inflammatory macrophages; Mo – monocytes; iMo - inflammatory monocytes; B – B-cells; T – T-cells and Nph – neutrophils. Statistic is 2-way ANOVA with Bonferroni's post-hoc test (* $p < 0.05$; ** $p < 0.01$; *** $p < 0.001$; # $p < 0.0001$; $n = 4$).

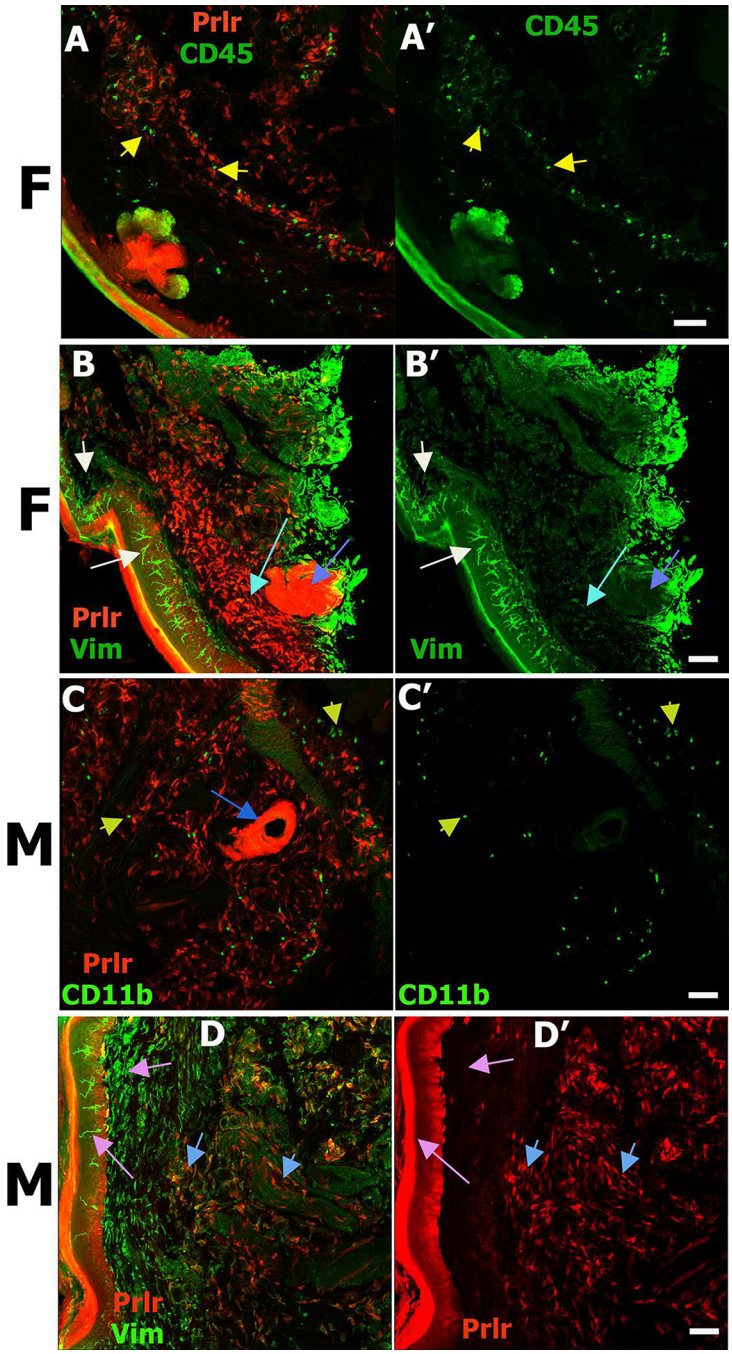

Fig. 11. Prlr mRNA expression in naïve female and male hind paw skin

Glabrous hind paw skin biopsies containing epidermis and dermis layers from naive $Prlr^{cre/-}/Rosa26^{LSL\text{-}tDTomato/-}$ female and male mice were dissected and cryo-sectioned for IHC. These cryo-sections from females (marked F) and males (marked M) showing Prlr-cre^{+} cells in red were co-labeled with **A-A'**: pan immune cell marker CD45; **B-B', D-D'**: pan fibroblast marker vimentin (Vim); **C- C'**: monocyte/macrophage marker CD11b; Yellow arrows show CD45^{+} (*panels A, A'*) and CD11b^{+} (*panels C, C'*) cells. A cyan arrow marks Vim^{+}/Prlr-cre^{+} cell (*panels B, B'*). White arrows show Vim^{+}/Prlr-cre^{-} cells (*panels B, B'*).

A blue arrow points to epithelial cells of sweat glands (*panels B, B'*). A blue arrow points to skin capillary vessels (*panels C, C'*). Light blue arrows point to Vim^{+}/Prlr-cre^{+} fibroblasts of the skin dermis layer (*panels D, D'*). Pink arrows show Vim^{+}/Prlr-cre^{-} cells of the skin epidermis/dermis layer (*panels D, D'*). Markers and their colors are noted within panels. The photomicrographs of fluorescent labeled cells were captured with 20X objective. Scale bar on every panel A'-D' is 30 μm.

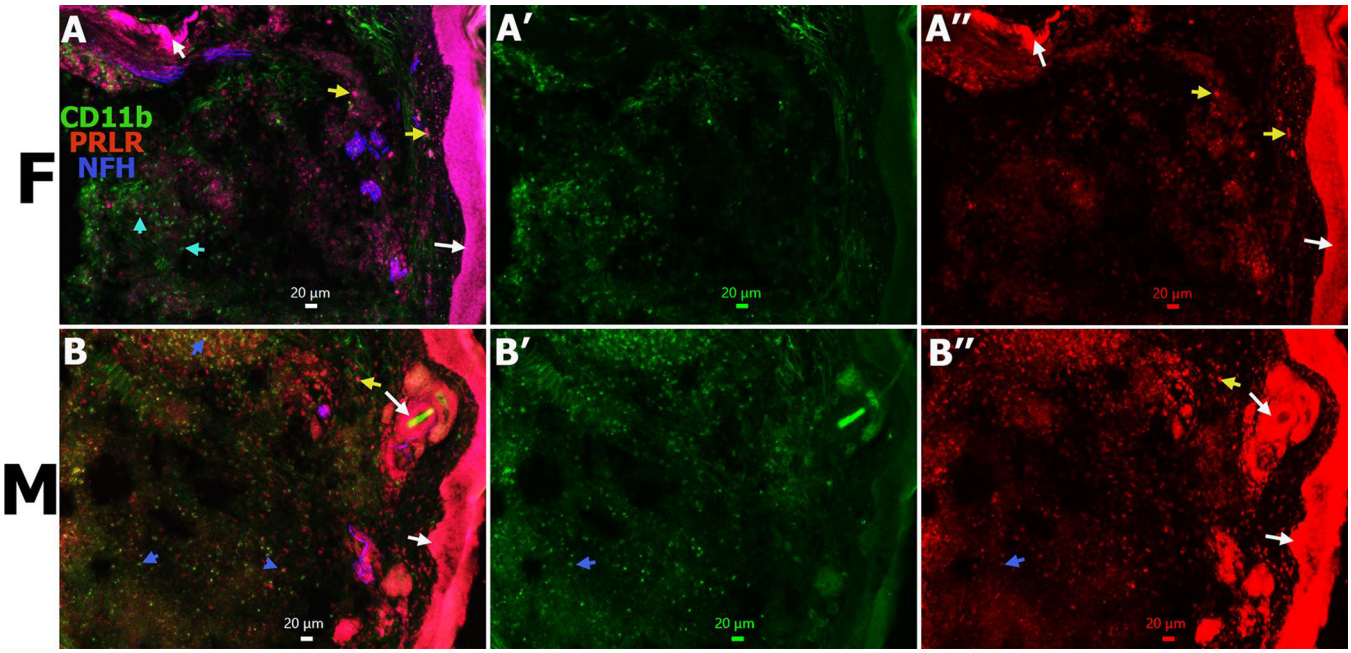

Fig. 12. PRLR expression in hind paw skin of CFA-treated females and males

Complete Freund's adjuvant (CFA) was injected i.pl. in males and females. Glabrous hind paw skin biopsies containing epidermis and dermis layers from these mice were dissected and cryo-sectioned for IHC. **A, B**: These cryo-sections from females (marked F, panels A-A") and males (marked M, panel B-B") were co-labeled with pan-myeloid cell marker CD11b (green), PRLR antibodies (red) and A-fiber marker NFH (blue). White arrows point to $PRLR^+$ epithelial cells of hair follicles and epidermis layer (*panels A, A", B, B"*). Yellow arrows point to dermis $PRLR^+/CD11b^-$ cells (*panels A, A", B, B"*). Blue arrows point to male dermis $PRLR^+/CD11b^+$ cells (*panels B-B"*). Cyan arrows show $PRLR/CD11b^+$ cells of the female skin dermis layer (*panel A*). Antibodies and their colors are noted within the panel A. The photomicrographs of fluorescent labeled cells were captured with 10X objective. Scale bar on every panel is 20 μm.